Modern developments in hypersonic wind tunnels

R. J. Stalker
Centre for Hypersonics
University of Queensland
Brisbane, Autralia

ABSTRACT

The development of new methods of producing hypersonic wind-tunnel flows at increasing velocities during the last few decades is reviewed with attention to airbreathing propulsion, hypervelocity aerodynamics and superorbital aerodynamics. The role of chemical reactions in these flows leads to use of a binary scaling simulation parameter, which can be related to the Reynolds number, and which demands that smaller wind tunnels require higher reservoir pressure levels for simulation of flight phenomena. The use of combustion heated vitiated wind tunnels for propulsive research is discussed, as well as the use of reflected shock tunnels for the same purpose. A flight experiment validating shock-tunnel results is described, and relevant developments in shock tunnel instrumentation are outlined. The use of shock tunnels for hypervelocity testing is reviewed, noting the role of driver gas contamination in determining test time, and presenting examples of air dissociation effects on model flows. Extending the hypervelocity testing range into the superorbital regime with useful test times is seen to be possible by use of expansion tube/tunnels with a free piston driver.

NOMENCLATURE

A_∞	test flow area
A_f	frontal area
A_p	planform area
C_L	lift coefficient = (lift) $\times$ 2/($\rho_\infty V^2 A_p$)
C_M	pitching moment coefficient = (pitching moment about balance centre) $\times$ 2/($\rho_\infty V^2 A_p Z$)
C_T	thrust coefficient = (forward thrust) $\times$ 2/($\rho_\infty V^2 A_f$)
D	test flow diameter
h_∞	free stream enthalpy, including dissociation energy
h_f	frozen enthalpy
h_s	streamline enthalpy
H	stagnation enthalpy
M_∞	free stream Mach number
M_c	precombustion Mach number
p	pressure
P_c	precombustion pressure
P_D	piston driver pressure
P_p	pitot pressure
P_R	nozzle reservoir pressure
R	gas constant for air (= 287 J/kg/K)

Paper No. 3025. Manuscript received 26 September 2005, accepted 19 October 2005.
This paper is the latest in a series of invited survey papers focusing on a specific aspect of the aeronautical industry.

https://doi.org/10.1017/S0001924000004346 Published online by Cambridge University Press

P_u unit Reynolds number
T_∞ free stream temperature
T_c precombustion temperature
u velocity downstream of shock
V free stream velocity
V_n equivalent velocity = $\sqrt{2H}$
W test flow power
x streamline distance downstream of shock
Z chord length
β angle between shock and free-stream velocity
γ ratio of specific heats
λ volumetric compression ratio of driver gas
ρ_∞ free stream density
ϕ equivalence ratio

1.0 INTRODUCTION

The development of hypersonic wind tunnels has been largely funded by governments, so it is not surprising that there should be periods of intense activity in between longer, relatively quiescent, periods as the perceived prospect of hypersonic flight advanced and receded.

The first period of activity occurred during the late 50s and through the 60s, and was spurred by the many design projects at the time which involved hypersonic flight, and the widespread feeling that theoretical knowledge of hypersonic flow phenomena was not fully developed. This period saw the construction of many 'cold' intermittent hypersonic wind tunnels, with test times of at least a few seconds, where hypersonic flow was produced by reducing the speed of sound of the airflow while adding as little energy as possible to increase its velocity[1]. At the same time, this period also saw the introduction of impulse wind tunnels[2,3,4], in which the hypersonic flow was produced by expansion of air from a high temperature reservoir, avoiding the problem of containment in the reservoir by operating with test times of a small fraction of a second.

The period encompassing the 70s to the mid 80s was an interval of relative quiescence. Nevertheless, stemming from the realisation that hypersonic propulsion was a critical field which was very poorly understood, this period saw attention to the development of intermittent wind tunnels, suitable for experiments on scramjet configurations. Research in these wind tunnels led to another period of intense activity, which occurred from the mid 80s into the 90s, when the National Aerospace Plane project in the USA, and the 'Hope' and 'Hermes' re-entry glider projects, in Japan and Europe respectively, encouraged the relatively rapid diffusion of the free piston shock tunnel.

Since the funding requirements of university research were relatively modest, it was not generally subject to perceptions of the immediacy of hypersonic flight, and core activities were able to continue in this sector at a more or less steady pace. Because impulse facilities could be acquired at modest cost levels, and operated reasonably economically, they tended to be favoured by the university community, and a considerable part of the continuing development of impulse facilities and techniques has taken place in the universities.

The term 'modern' which appears in the title covers the last few decades, since it is during this time that the hypersonic wind tunnel concepts which are the subject of the review appeared and were developed. In general, these concepts were directed to increasing the test section velocity in hypersonic wind tunnels, and the review will follow this trend, while noting the importance of other considerations. Wind tunnels for hypersonic propulsion experiments will be considered in a separate category to those for hypervelocity aerodynamic experiments but, as will become apparent below, there is considerable overlap between the two.

The review begins with a discussion of the simulation requirements of wind tunnels in the two categories of hypersonic propulsion and of hypervelocity aerodynamics. It then goes on to consider developments in intermittent hypersonic wind tunnels, noting the importance of reservoir pressures and test section size. Impulse facilities are discussed next, with special regard to the variety of operating techniques and developments in instrumentation as well as their relation to airbreathing flight propulsion. Finally, the use of impulse wind tunnels at superorbital test velocities is noted, together with the results of early experiments.

2.0 HYPERSONIC SIMULATION

As well as their role in representing flight flow fields, wind tunnels can be used for basic research on the physics of flow situations, and the emphasis is then on experimental design which will reveal that physics. However, even in this case, the utility of a wind tunnel depends on its ability to supply flow conditions which are representative of the phenomena to be investigated. Thus, as with the representation of flight flow fields, the capacity of a wind tunnel to simulate flight conditions is of fundamental importance.

The first step in simulating hypersonic flows was to simulate high Mach number effects with low stream temperature (i.e. 'cold') hypersonic wind tunnels. The last few decades have seen improvements in flow quality, Reynolds number capability and instrumentation techniques with such wind tunnels (e.g. Refs 5 and 6), but they have remained limited to flow speeds of about 1·5kms^{-1}. Interest in flight at higher speeds demanded the development of hypersonic wind tunnels which could provide simulation of flow fields at these speeds, where the increased flow energies yielded temperatures at which chemical reactions were an important feature of hypersonic flow fields. New developments in hypersonic wind tunnels during the last three or four decades have largely been directed towards producing test flows at these higher speeds. These wind tunnels may be described as 'thermo-hypersonic', signifying the importance of high temperature effects in the flow fields they produce, or as 'sub-orbital hypersonic', implying that they produce flow speeds which are a significant fraction of Earth orbital velocity. The term 'hypervelocity' is more generally used and describes wind tunnels which produce flow speeds in excess of 3kms^{-1}. The problems of flow field simulation in these wind tunnels depends on whether a propulsive or an aerodynamic flow field is involved.

2.1 Simulating propulsive flow fields

The lowest speeds at which chemical reactions become an important part of the flow field are about 2kms^{-1}, where scramjet propulsion becomes of interest. Airbreathing flight propulsion at lower speeds normally involves turbojets or ramjets, where the chemically reacting part of the flow is essentially independent of the general flow field, and therefore does not need to be part of the overall flow simulation. However, scramjets require integration with the flow field about a vehicle configuration, and therefore flow field simulation must involve the chemical reactions of the combustion process.

Therefore, simulation involves producing the conditions in a scramjet wind tunnel model which will allow the combustion reactions to reach the same degree of completion as in the equivalent flight configuration. This requires a relation for scaling between combustors of different sizes. shock tunnel experiments with simple, rectangular, constant area, combustion ducts, with fuel injection from a strut mounted in the mid-plane of the duct[7,8,9], have shown that such combustors follow a binary scaling relation, implying that, for geometrically similar combustors

$$P_c L_c = \text{constant} \sim 2 \times 10^4 \text{ Pa.m.} \quad \ldots (1)$$

Where P_c is the precombustion pressure in the combustor, and L_c is its length. The numerical value of the constant at the right hand side

https://doi.org/10.1017/S0001924000004346 Published online by Cambridge University Press

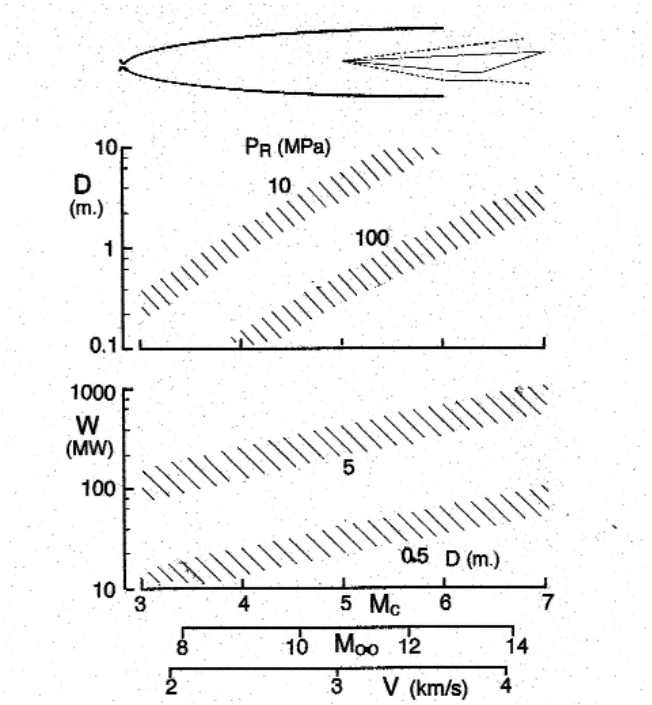


Figure 1. Approximate requirements for simulation of propulsive flow fields (D = test flow diameter, P_R = nozzle reservoir pressure, M_C = precombustion Mach number, M_∞ = free-stream Mach number, V = free stream velocity).

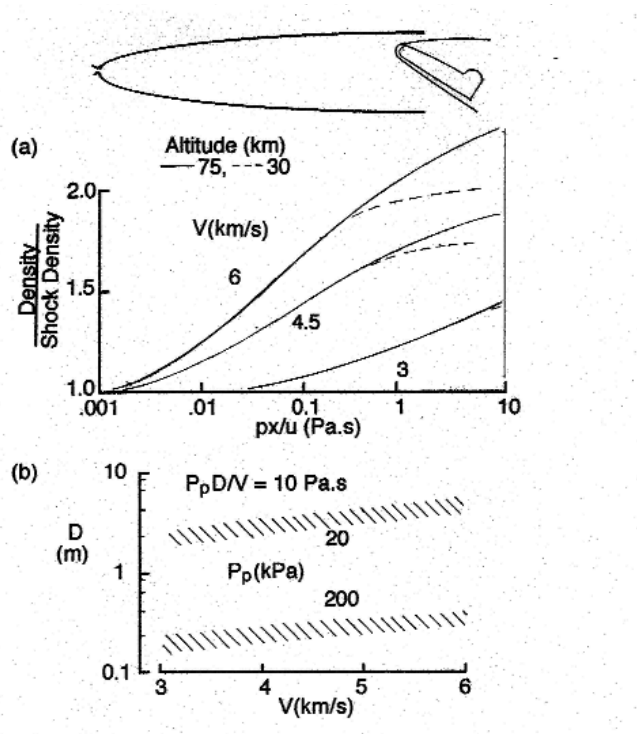


Figure 2. Binary scaling and hypervelocity simulation
(a) Constant pressure relaxation after shock
(p = post shock pressure (Pa), u = post shock velocity (m/s), x = distance from shock (m), V = free-stream velocity).
(b) Simulation of hypervelocity flow fields.
(P_P = pitot pressure, D = test flow diameter).

of Equation (1) may vary as parameters such as the precombustion Mach number are varied, and may change for different combustion configurations. However, Equation (1) is useful as a means of exploring the limits of hypersonic wind tunnels in simulating hypersonic propulsive flow fields.

Though the detail of the model configuration will determine the relation between model size and combustor length, the fact that a low drag hypersonic configuration will be required to ensure reasonably efficient propulsion will ensure that a slender configuration is required, with an overall length some ten times the combustor length. The test flow diameter of a hypersonic wind tunnel may be about one third of the model length, as shown, for example, in the sketch at the top of Fig. 1, and therefore may be taken as three times the combustor length. Now, the test flow will normally be supplied by a steady hypersonic nozzle expansion and subsequent recompression in the model intake to the precombustion Mach number, M_c, and assuming that both are isentropic, the precombustion pressure is given by

$$P_c = P_R \left\{1+0{\cdot}5(\gamma-1)M_c^2\right\}^{-\gamma/(\gamma-1)} \quad \ldots (2)$$

where P_R is the nozzle reservoir pressure. Thus, using Equation (1), with $3L_c \sim D$, the test flow diameter, it follows that

$$P_R D \sim 0{\cdot}06\left\{1+0{\cdot}5(\gamma-1)M_c^2\right\}^{\gamma/(\gamma-1)} \text{ MPa.m.} \quad \ldots (3)$$

where P_R is measured in MPa. Taking γ = 1·35, this approximate relation is presented in Fig. 1 for selected values of the nozzle reservoir pressure. Cross hatched zones are used to indicate that the relation is indeed an approximate one but, nevertheless, it serves to illustrate the nexus which exists between wind tunnel size and the pressure levels required for simulation of a scramjet flow field in a hypersonic wind tunnel. Of course, the limits imposed by this nexus can be extended for experiments on components of a scramjet but, in this discussion, only simulation of the complete vehicle flow field is considered.

The binary scaling relation of Equation (1) also has implications for the wind-tunnel power levels required for simulation of propulsive flow fields. The test section power level, W, is, to a good approximation, obtained by taking the product of flow kinetic energy per unit area and the mass flow to yield.

$$W = 0{\cdot}5\rho_\infty A_\infty V^3 \quad \ldots (4)$$

where ρ_∞, A_∞ and V are the test section density, cross sectional area and velocity respectively. With the assumption of isentropic compression in the scramjet intake, and a perfect gas equation of state,

$$\rho_\infty = \left(P_c/RT_c\right)\left(T_\infty/T_c\right)^{1/(\gamma-1)} \quad \ldots (5)$$

The value of the precombustion temperature, T_c, at which ready ignition of a stoichiometric mixture of hydrogen and air will readily ignite is taken as approximately 1,000K which, since simulation of the intake compression is required, is approximately four times T_∞. From Equations (2) and (3)

$$P_c D \sim 6 \times 10^4 \text{ Pa.m.}$$

and, using Equation (5), as well as putting $A_\infty = \Pi D^2/4$, Equation (4) yields

$$W \sim 1{\cdot}6DV^3 \text{ MW} \quad \ldots (6)$$

https://doi.org/10.1017/S0001924000004346 Published online by Cambridge University Press

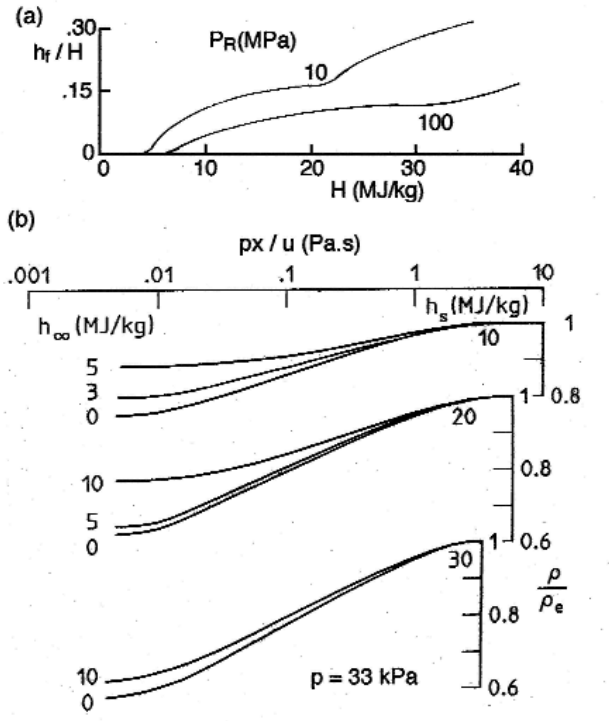


Figure 3. Nozzle freezing of chemical dissociation.
(a) Frozen fraction of stagnation enthalpy.
(h_f = frozen dissociation enthalpy (MJ/kg), H = stagnation enthalpy (MJ/kg), P_R = nozzle reservoir pressure).
(b) Constant pressure relaxation with upstream freezing. (px/u = binary scaling parameter, h_∞ = upstream enthalpy, h_s = streamline enthalpy, ρ_e = equilibrium density).

where V is in kms^{-1} and D in metres. This relation is presented in Fig. 1 for selected values of the test flow diameter, the approximate nature of the relation being once again recognised by the use of cross hatched zones. Scales of test section Mach number and velocity corresponding to the precombustion Mach number are also shown in the figure.

Figure 1 displays the increasing difficulty associated with simulating propulsive flow fields as Mach number is increased. For example, to increase the Mach number by 50% requires either a factor of ten increase in the tunnel size, or in the nozzle reservoir pressure, and an increase in test section power levels by a factor of three. As a consequence, very large wind tunnels operating at high nozzle reservoir pressures and high power levels are required at high Mach numbers. Add to this the problems of heat transfer to tunnel components (and to the models) due to the high flow energies involved and it becomes clear that high Mach number simulation of propulsive flow fields will be inhibited by severe engineering difficulties.

2.2 Simulating hypervelocity aerodynamic flow fields

Evidence of chemical reactions begins to appear in aerodynamic flow fields as velocities exceed 3kms^{-1}, and for this reason the term 'hypervelocity' was coined to cover hypersonic flows at such velocities. The flight vehicle configurations considered for operation in this regime have, up to the present, involved a relatively blunt shape on the windward side, as shown at the top of Fig. 2. Thus the flow field about the vehicle will be preceded by a strong shock. There may be future applications which involve slender, low drag, aerodynamic configurations, such as orbital plane change vehicles, and the flow about such vehicles would not necessarily be preceded by a strong shock. Simulation of such flow fields will not be considered here.

Binary Scaling

When the air crosses the strong bow shock high temperatures are generated and dissociation of the air molecules begins. Dissociation continues as the air passes downstream with the result that the temperature reduces and, for a constant pressure flow, the density increases. This is shown in Fig. 2(a), where the ratio of the density immediately downstream of the shock is plotted against a parameter consisting of the product of the pressure, representing the density dependence of the dissociation rate, and the time for which the dissociation reactions proceed[10]; i.e. a binary scaling parameter. The curves in the figure apply to the flow downstream of a normal shock, but they can be used for a strong oblique shock by taking V as the freestream velocity normal to the shock, and x and u as the distance and velocity along a streamline downstream of the shock. Curves are presented for flight altitudes of 75km and 30km, the corresponding ambient densities differing by a factor of approximately 450. The curves are identical up to the point where the 30km curves trend to the equilibrium condition, where dissociation is balanced by recombination. As altitudes are increased to 75km this departure point occurs at higher values of px/u. The coincidence of the curves for widely differing densities indicates that binary scaling applies to the non-equilibrium flow downstream of a strong bow shock, until it approaches equilibrium.

Thus, when binary scaling applies, dissociating flow fields at a given velocity can be simulated in a hypersonic wind tunnel by matching the value of the binary scaling parameter – i.e. by matching the product of a reference pressure and a flow field reference dimension. However, the value of the binary scaling parameter should be such that the approach to equilibrium is avoided in the tunnel as well as in the flight flow fields. Because of the small model scale, the tunnel will require higher pressures than flight, and hence higher densities, for matching of the flight binary scaling parameter, and these higher densities will cause an approach to equilibrium at lower values of the binary scaling parameter. The same effect is evident in Fig. 2(a), where the higher densities corresponding to the lower altitude cause an approach to equilibrium at lower values of the binary scaling parameter.

For example, with a vehicle 30m long, at an angle of incidence of 45°, a velocity of 6kms^{-1}, and an altitude of 67km (representing the NASA Space Shuttle), the value of px/u is 16. The curve at 4·5kms^{-1} in Fig. 2(a) then shows that although the flight vehicle flow on the windward side is only beginning to approach equilibrium, the increase in density associated with increasing the pressure to compensate for the reduced length of a wind tunnel model implies that the model flow approaches equilibrium at smaller values of px/u. The effect on density is small, but the streamwise rate of variation of the density is affected more, which may lead to small, but important, effects such as a shift in the centre of pressure[11]. Thus, provided that the chemical composition of the tunnel freestream matches that in flight, binary scaling may be used as a basis for simulation of flight flow fields, with some reservations concerning flow field details associated with an approach to equilibrium in the tunnel flow field.

Taking the pitot pressure, P_p, as the reference pressure, with the length of the model as the reference dimension, and putting the length of the model equal to the test flow diameter, D, a relation between the pitot pressure and the test diameter is obtained. This relation is presented in Fig. 2(b) for $P_pD/V = 10$Pas and two values of the pitot pressure. The approximate nature of the relation is again represented by cross hatching. Figure 2(b) shows the favourable effect of wind-tunnel size. Increasing the size allows a decrease in test flow pressure levels and therefore allows binary scaling to be applied for greater downstream distances from the bow shock.

As noted in Section 2.1, the maximum nozzle reservoir pressure is an important performance parameter for hypersonic wind tunnels. The relation between nozzle reservoir pressure and the pitot pressure of Fig. 2(b) depends on the test section Mach number and, when the flow field to be simulated is preceded by a strong shock,

https://doi.org/10.1017/S0001924000004346 Published online by Cambridge University Press

the Mach number loses its importance as a simulation parameter, by virtue of the Mach number independence principle. This has been stated by Hayes and Probstein[12] as follows: '*The flow around a body behind the bow shock depends only on the density and uniform velocity of the gas in the free stream…*'. In view of the discussion below on the effect of free stream dissociation freezing, it should be noted that this applies when the chemical composition of the free stream is fixed. The important point to note at this stage is that, for a satisfactory simulation, it is not necessary to expand the test flow to the correct Mach number, provided that the Mach number is sufficiently high to produce a strong bow shock. Thus the relation between the pitot pressure and the nozzle reservoir pressure is somewhat arbitrary. For example, for a nozzle expansion with $\gamma = 1{\cdot}35$ a pitot pressure, P_P, of 20kPa corresponds to a nozzle reservoir pressure, P_R, of 2MPa at a test Mach number of 7·3, and to a value of P_R of 10MPa at a Mach number of 9·9, while for a value of P_P of 200kPa, these values of P_R are increased by a factor of 10.

Nozzle freezing

For hypervelocity flow, the nozzle reservoir is at temperatures which are sufficiently high to dissociate some or all of the molecular species of air into atoms, and some of these atoms fail to recombine in the expansion. This yields a test section flow in which some of the dissociation reactions are 'frozen' and the free stream enthalpy therefore includes the dissociation energy of these reactions. Atmospheric air contains almost no frozen species, and this gives rise to a difficulty in simulating hypervelocity flight.

The proportion of the flow stagnation enthalpy consisting of frozen dissociation energy, obtained from the correlation of Harris[13], is shown in Fig. 3(a) for a nozzle area ratio of 1,000 and two values of the nozzle reservoir pressure. The proportion of stagnation enthalpy due to frozen dissociation energy increases and approaches a plateau as the frozen oxygen dissociation proceeds to completion, then increases again as substantial frozen nitrogen dissociation occurs. Frozen dissociation energy represents as much as 30% of the stagnation enthalpy at high stagnation enthalpies when $P_R = 10$MPa, but falls to approximately half that value for $P_R = 100$MPa. Reference 13 indicates that varying the size of the nozzle does not have a large effect on dissociation freezing implying that, for minimising frozen dissociation, high operating pressures have an advantage over large size. This needs to be checked with more calculations involving nozzles of varying size but, as it stands, it is in contrast to the requirement for binary scaling noted above, where large size was advantageous.

The presence of frozen dissociation energy in the test flow changes density ratios across the bow shock. Assuming Newtonian flow and instantaneous post shock equilibrium, it can be shown that, for a shock making an angle β with respect to the free stream, the shock density ratio is reduced by a factor of approximately $\{1 - h_f/(H\mathrm{Sin}^2\beta)\}$. Thus a reduction which is comparatively small when the shock is normal to the free stream can become a large reduction when the shock angle is reduced.

Of course, the post shock flow does not instantaneously reach chemical equilibrium and, because frozen dissociation changes conditions immediately downstream of the shock, the rate at which the flow reacts and approaches equilibrium is changed. The effect of this is displayed in Fig. 3(b), where the approach of density to an equilibrium value with increase in the binary scaling parameter, px/u, is shown. The upstream enthalpy includes the frozen dissociation energy and the figure shows that, when this is less than approximately one third of the streamline enthalpy, the density variation is close to that obtained with zero upstream enthalpy. It might be noted that, as before, the effect of upstream dissociation will be less evident for a normal shock than an oblique one, since the streamline enthalpy is reduced for an oblique shock while the upstream enthalpy remains the same, thus ensuring that the upstream enthalpy is a greater proportion of the streamline enthalpy.

Therefore free stream dissociation freezing has a relatively small effect when the bow shock is not too far from being normal to the oncoming flow, but has a larger effect for small shock angles. Taking these effects into account in simulations involving both blunt bodies and the flow over straight surfaces with moderate values of the shock angle is discussed in Ref. 14. For curved shocks which are not nearly normal to the freestream flow, quenching of the dissociation reactions occurs downstream of the shock, as explained qualitatively in Ref. 14, and the consequences of this effect for simulation of attendant flow fields have not been explored. Thus, although it is possible to develop similitudes for some configurations, (or parts of configurations) with freestream dissociation freezing, the problem of creating general similitude rules remains unresolved.

2.3 Binary scaling and Reynolds number

Both propulsive flow fields and hypervelocity flow fields rely on binary scaling for simulation. But simulation of the boundary layers in a flow field demands matching of the Reynolds number as well. In the absence of free-stream dissociation freezing, the freestream velocity, temperature and viscosity are fixed at any given stagnation enthalpy, and matching of the binary scaling parameter ensures that, in addition, the product of freestream density and a characteristic dimension is matched. Thus the freestream Reynolds number is matched and, in view of the flow field matching, so is the post shock Reynolds number.

The situation is less clear when substantial freestream dissociation freezing is present. This has only a small effect on the freestream Reynolds number but, because there may be substantial effects of freezing on the post shock flow, there may also be significant effects on post shock Reynolds numbers.

3.0 INTERMITTENT PROPULSIVE WIND TUNNELS

Hypersonic propulsion is probably the area of hypersonics most in need of research and development effort in the near future[15], not least because of the extreme demands on wind tunnels at high Mach numbers implied by Fig. 1. Of course, these demands arise in the context of simulation involving complete configurations, and they are considerably eased if the behaviour of components of these configurations are studied in isolation. Indeed, this type of combustion research has been widely used in research on supersonic propulsion, and it would be surprising if the study of hypersonic propulsion did not benefit from the same approach.

3.1 Combustion Heating

An example of a hypersonic facility for study of components of propulsive configurations is shown in Fig. 4, which is a representation of the blowdown tunnel laboratory described in Ref. 16. The facility is supplied with air from a tank farm of volume 100m^3, and exhausts to the 1,600m^3 volume vacuum sphere shown in the figure, providing test times of up to 10 minutes as required. There are five test legs, numbered from left to right in Fig. 4 as I to V. The five legs employ heating of the airstream by combustion of hydrogen, with make-up oxygen added to produce a vitiated airstream. Thus, the test gas is an air-like mixture, with a high fraction of combustion products.

Legs I and II are used for simulation of the combined combustor-thrust nozzle component of a scramjet engine, and this allows direct supply of test gas from the wind-tunnel nozzle, without the wind tunnel nozzle expansion and subsequent inlet compression which would be required for a complete engine. These legs operate up to a nozzle reservoir pressure and temperature of 12MPa and 2,500K respectively. Referring to Fig. 1, the nozzle reservoir pressure, with

https://doi.org/10.1017/S0001924000004346 Published online by Cambridge University Press

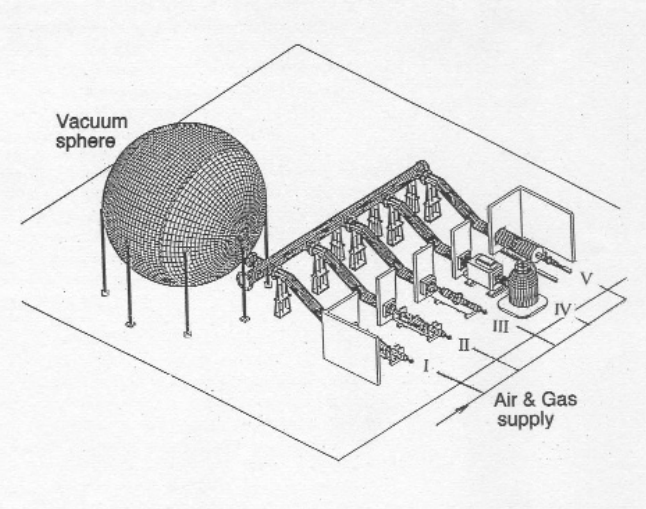


Figure 4. Blowdown laboratory for hypersonic propulsion.

a combustor length of 1m, allows operation up to a precombustion Mach number, M_c, near 5 but, with a precombustion temperature of 1,000K, operation is possible only up to a precombustion Mach number somewhat in excess of 3, thereby simulating a flight free stream Mach number approaching 8. Thus the reservoir temperature limits the flight Mach number at which simulation is possible, rather than the binary scaling relation.

Leg III is a duct with a rectangular cross-section, 19mm × 32mm, which is used for testing samples of materials and structural elements. It operates at reservoir pressures up to 8·2MPa and reservoir temperatures up to 2,700K, with heating provided by hydrogen or ethylene combustion.

Legs IV and V are free jet facilities used for complete engine testing. Leg IV incorporates a pebble bed heater which provides dry air at a temperature of 1,300K and, with hydrogen combustion heating as well, provides vitiated air at reservoir temperatures of approximately 3,000K. Reservoir pressures are limited to 10MPa. As for legs I and II, the reservoir temperature limits the flight Mach number at which simulation is possible to values between 8 and 9. Leg V is unique in that the supersonic/hypersonic nozzle, reservoir and heater are mounted to rotate with respect to the stationary model axis, allowing the flow from the nozzle to pass through an oblique shock formed by a flat plate upstream of the model before passing into the model intake. By rotating the nozzle assembly during a test the continual variation of model inlet conditions, as would be experienced by an engine mounted on an accelerating vehicle, can be simulated. Leg V does not incorporate an upstream pebble bed heater, but employs hydrogen combustion to provide vitiated air at a reservoir temperature and pressure of 2,500K and 12MPa.

The use of a range of wind-tunnel types to test components of a complete scramjet configuration is also evident in the review of scramjet research at the NASA Langley Research Centre[17], where direct connect facilities with vitiated air heated by combustion of hydrogen are also used for scramjet research. The same method of heating is used in free jet wind tunnels, which are used for testing of complete model engines up to a simulated flight Mach number of 6. These facilities are supplemented by an arc heated hypersonic wind tunnel in which extra air is added downstream of the arc, and this provides an 0·28m square section test flow up to a flight Mach number of 8. A virtue of the facility is that, although it has its own test flow contamination problems, they are not the same as combustion heated facilities, indicating that comparison of results between the two types of facility can reveal contamination effects in either or both.

A hypersonic, combustion heated wind tunnel with a 2·4m diameter test flow is also described in Ref. 17. This was originally designed as a thermo-structural facility, heated by combustion of methane, and was modified by the addition of an oxygen replenishment system to become a hypersonic propulsion wind tunnel. It can provide stagnation temperatures of 2,000K at nozzle reservoir pressures of 13MPa which, referring to Fig. 1, would correspond to a precombustion Mach number of 5 and a free-stream Mach number of 11, with model lengths of the order of 10m. However, the stagnation temperature limits simulation to a free-stream Mach number of 6·8. Also, the test cabin does not allow such large models. If, in order to avoid choking, it is necessary to inject models into the test flow after the flow has started, the model length is limited to 3·7m. Otherwise, somewhat larger models could be tested.

It is worth noting that the facilities described up to this point were employed for development of the successful NASA 'Hyper-X' flight of March 2004, in which a scramjet, in a model vehicle 3·7m long, provided propulsive thrust at Mach 7 for 7 seconds.

A facility capable of testing scramjet engines at their expected full size is the Aerodynamic and Propulsion Test Unit at the Arnold Engineering Development Centre[18]. This is currently being upgraded with a new combustion heater and a Mach 7 nozzle to produce a 1·1m diameter test flow with a stagnation temperature of 2,600K and a nozzle reservoir pressure of 19MPa, allowing simulation up to a flight Mach number of 8. The upgrade plans include mounting the heater and nozzle on a stand which can be rotated during a test, similar to the arrangement described above, thus allowing testing of a full scale engine in an accelerating phase of flight. This facility is being developed in an environment with several decades of experience in the development testing of large aircraft engines, and therefore considerable attention is being given to instrumentation and control issues.

It may be pointed out that facilities which employ combustion heating use a test gas which is not air. However, as noted in Ref. 18, '*… the ability to construct and operate a facility safely and affordably (is) a very real issue. Realistically, sacrifices in simulation parameters are made with the realization that increased uncertainty in the test data will result.*' Recent scramjet powered flight tests have reduced this uncertainty and, because the test times of many seconds makes these facilities suitable for many purposes for which no alternative is available, such as tests involving materials and other thermo-structural phenomena, they can be expected to continue to play an important part in the development of hypersonic propulsion.

3.2 Ultra high pressure and electron beam heating

Combustion heating limits intermittent propulsive wind tunnels to Mach numbers of approximately 8. Electrical arc heated wind tunnels have been widely used for materials testing, but are confined to supersonic Mach numbers because of the difficulties associated with maintaining the integrity of a reservoir with arc heating at moderately high pressures. As already mentioned, arc heating is possible when accompanied by dilution with air, but this is also limited to Mach numbers of 8. This 'Mach 8 barrier' has encouraged research on a new type of intermittent hypersonic wind tunnel known as a radiatively driven hypersonic wind tunnel (RDHWT)[19]. This type of wind tunnel has not yet been built, but it is useful to briefly review the concept, as it is a novel approach involving a number of interesting physical effects.

The problems involved in achieving the high velocities necessary to high Mach number flight simulation in a conventional intermittent wind tunnel are related to heat transfer. First, the reservoir enthalpies which are necessary at the reservoir pressures involved are such that heat transfer makes containment impossible, and second, excessive heat transfer to the throat and walls of the nozzle in the presence of air makes their survival unlikely.

https://doi.org/10.1017/S0001924000004346 Published online by Cambridge University Press

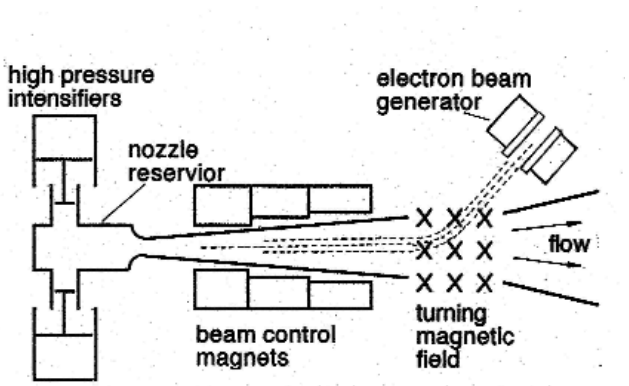


Figure 5. Ultra high pressure electron beam heated hypersonic wind tunnel – Schematic.

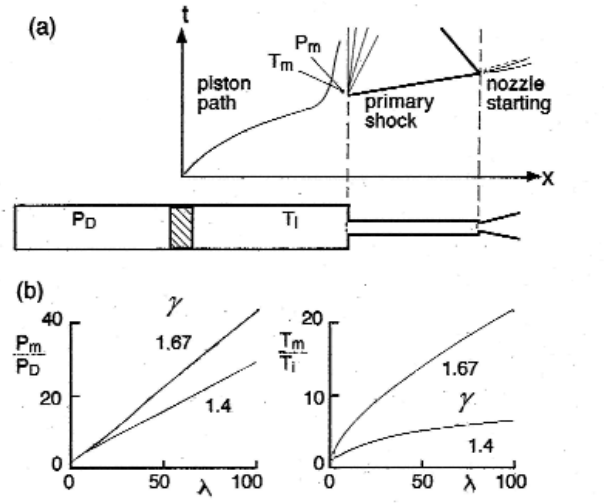


Figure 6. Free piston shock tunnel operation.
(a) Wave diagram showing shock tunnel operating cycle (P_D = initial pressure in piston driver reservoir, P_m, T_m = shock-tube driver pressure, temperature, T_i = initial temperature of shock-tube driver gas).
(b) Pressure and temperature amplification (λ = volumetric compression ratio of shock-tube driver gas, γ = ratio of specific heats).

The first of these problems is avoided by arranging that a substantial portion of the energy required (about two thirds) is to be added in the supersonic/hypersonic nozzle by means of a high energy electron beam, and by noting that as reservoir pressures are increased beyond 100MPa the volume occupied by the molecules of air, and the attractive force between them, become increasingly significant. As a result, the enthalpy becomes an increasingly strong function of pressure, a stagnation enthalpy of 2·5MJ/kg being obtained at a reservoir pressure of 2,000MPa and a temperature of 750K. In principle, with the reservoir walls at the same temperature, no heat transfer to the walls of the reservoir takes place. The energy addition in the nozzle is illustrated in Fig. 5. The electron beam is introduced at a station in the downstream part of the nozzle, and the flow is heated by collisional absorption of the beam energy. Numerical simulations[20] indicate that, by controlling the nozzle profile and the current distribution in the electron beam it is possible to produce a reasonably uniform core of flow at high enthalpy surrounded by a cooler wall layer. This central core can be expanded downstream of the heating region to produce the required test conditions.

The second problem, involving heat transfer to the throat and nozzle, is approached through film cooling, by injecting a wall layer of nitrogen in the reservoir. This is expected to be particularly effective in preserving a low enthalpy, non-oxidising layer adjacent to the wall, because the density is primarily dependent on the pressure (rather than the combination of pressure and temperature) at the ultra high pressures of the reservoir, implying that the nitrogen can be injected at the same pressure but a lower enthalpy than the air while keeping the densities of the two gases approximately the same. This causes the acceleration of the nitrogen layer and air to be the same in response to pressure gradients, with the result that there is a very small difference in the velocity of the air and the nitrogen as they pass from the reservoir, through the throat and into the supersonic region of the nozzle. As mixing between nitrogen and air at the interface between the two depends on this velocity difference, the mixing layer will grow very slowly, and the cool nitrogen layer will retain its integrity, and will protect the wall as it passes downstream.

Supplying air at a nozzle reservoir pressure of 2,000MPa involves meeting some novel engineering challenges[21] which, as illustrated schematically in Fig. 5, are being met by using an array of ultra high pressure intensifiers robustly coupled to an ultra high pressure manifold.

4.0 IMPULSE PROPULSIVE WIND TUNNELS

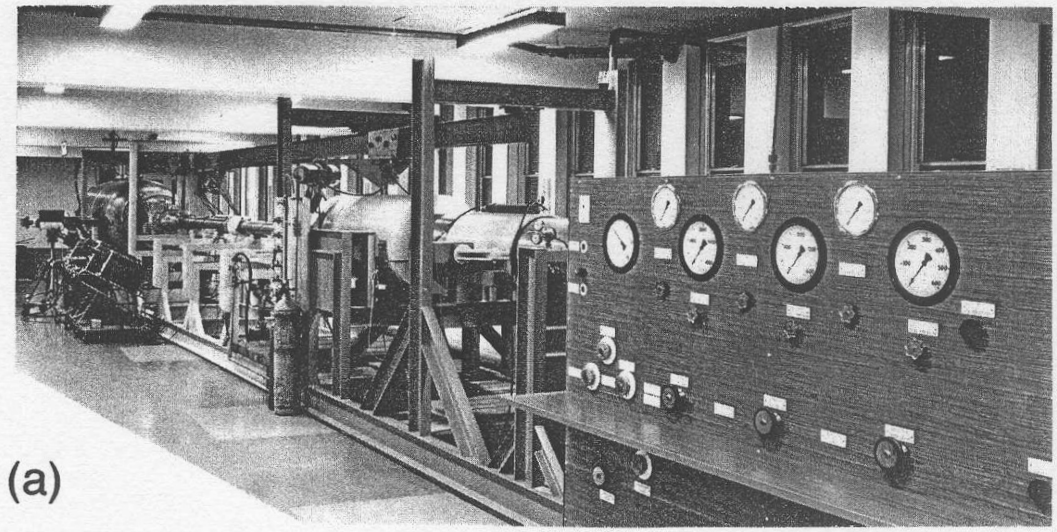
The maximum stagnation enthalpies of operating intermittent wind tunnels are limited by combustion heating to values which allow flight simulation up to Mach numbers near 8. Impulse facilities are not subject to this limitation, and therefore are able to provide simulation to much higher Mach numbers. Their disadvantage stems from the short duration of flows which they produce, with test times limited to only a few milliseconds. Thus, although they are suitable for simulation and study of aerodynamic and gas dynamic effects, they cannot be used to investigate other aspects of hypersonic flight, such as thermo-structural effects. That said, it should also be pointed out that aerodynamics and gas dynamics are of prime importance to a flight vehicle, and this gives impulse tunnels their particular legitimacy.

4.1 Free piston reflected shock tunnels

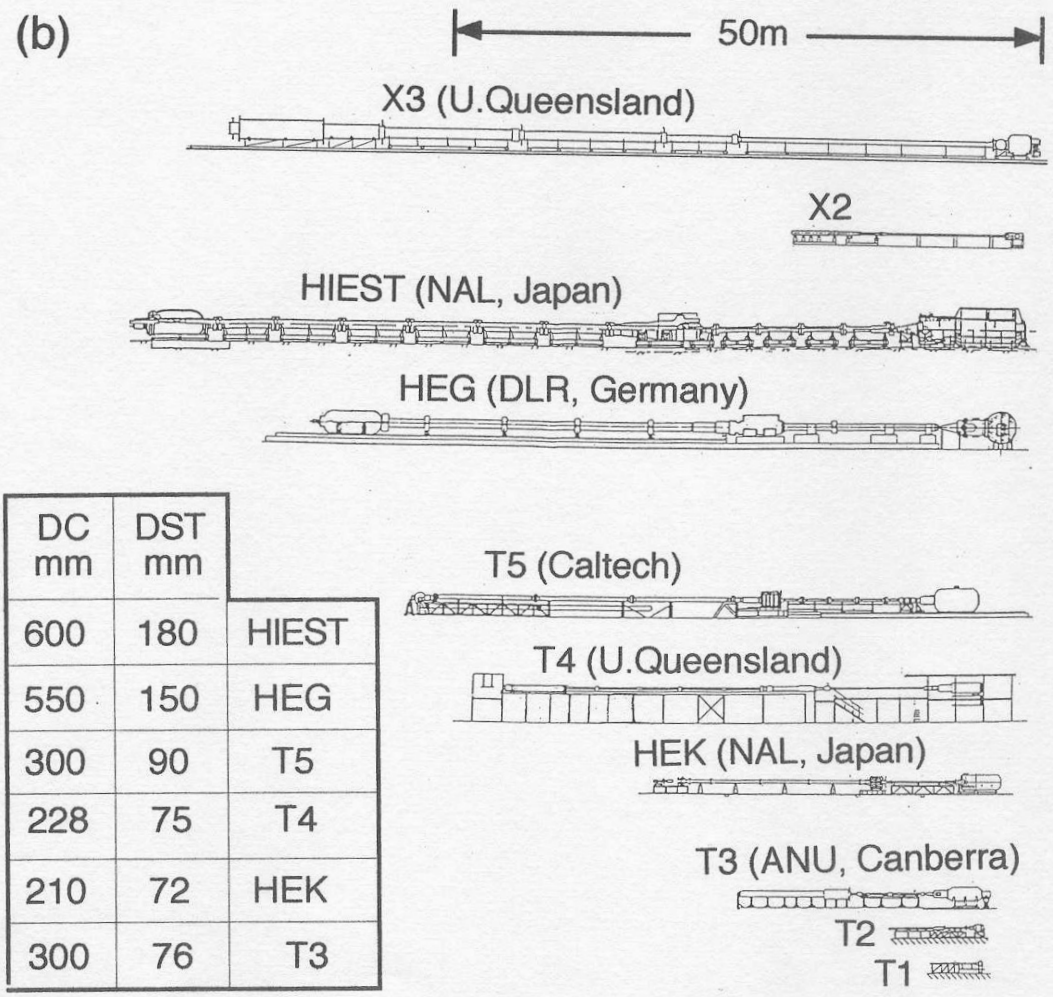
The reflected shock tunnel, which is used for hypersonic propulsive research, is the most widely used of the impulse facilities. Early research[22,23] showed that reflected shock tunnels could be used for studies of supersonic combustion, but a shock tunnel based continuing program of basic research on scramjet propulsion only began in the 80s, using the free piston shock tunnels T3 at the Australian National University, and T4, at the University of Queensland.

The operating cycle of a free piston shock tunnel is shown by the wave diagram in Fig. 6(a). This piston, which is represented by the cross-hatched rectangle in the figure, initially is subject to a much higher pressure, P_D, in the piston driver reservoir (on the left of the figure) than the initial pressure in the shock-tube driver gas (on the right of the piston in the figure). Thus, when it is released, the piston accelerates to the right but, as it approaches the entrance to the shock tube, the compression of the driver gas causes the piston to slow down. However, at a predetermined point in this compression process, before the piston comes to rest, the diaphragm at the entrance to the shock tube ruptures, and the driver gas expands into the shock tube to initiate the shock-tunnel cycle. The velocity of the piston is such that the flow of driver gas into the shock tube is matched by movement of the piston face, thereby ensuring that the pressure, P_m, and the temperature, T_m, of the driver gas at the

https://doi.org/10.1017/S0001924000004346 Published online by Cambridge University Press



(a)



DC mm	DST mm	
600	180	HIEST
550	150	HEG
300	90	T5
228	75	T4
210	72	HEK
300	76	T3

Figure 7. Free Piston Impulse Tunnels.
(a) Free piston shock tunnel T3.
(b) Growth of free piston shock tunnels and free piston expansion tubes (DC = compression tube diameter, DST = shock tube diameter).

https://doi.org/10.1017/S0001924000004346 Published online by Cambridge University Press

entrance to the shock tube remain constant for long enough to ensure a conventional shock-tunnel cycle.

The free piston technique offers two benefits, which are made evident by reference to Fig. 6(b). The curves presented in that figure were obtained by assuming that the expansion of the piston driver gas and compression of the shock-tube driver gas are both isentropic, and by taking the initial volumes of both gases to be equal. The amplification of shock-tube driver gas temperature, which is evident on the right hand side of the figure, allows the shock tunnel to generate stagnation enthalpies in the nozzle test flow which are well in excess of those available with combustion heated intermittent wind tunnels. As shown by the left hand side of the figure, the temperature amplification is associated with a pressure amplification, leading to a shock-tube driver pressure which becomes, at moderate values of the driver gas volumetric compression ratio, an order of magnitude greater than the initial pressures anywhere in the assembly.

These two pressure and temperature related benefits are partially offset by the reduced size of the shock tube and nozzle in comparison with the rest of the assembly, as this leads to a reduced test flow diameter. However, in practice, the shock tube diameter, which is related to the test flow diameter at any given Mach number, is approximately one third of the diameter of the tube in which compression of the driver gas takes place, whereas the pressure is increased by an order of the magnitude by the compression process. Figure 1 indicates that reducing the test flow diameter by a factor of three and increasing nozzle reservoir pressures by an order of magnitude increases the Mach number for propulsive simulation, thereby signifying that the use of free piston compression of the shock-tube driver gas increases the Mach number for propulsive simulation.

Examples of free piston facilities are shown in Fig. 7. Figure 7(a) is a photograph of the free piston shock tunnel T3 at the Australian National University, in Canberra. It was brought into operation in 1968[24] and has since been operating continuously, largely serving as a vehicle for university research. It was the first free piston shock tunnel of a substantial size to be built but, as shown in Fig. 7(b), much larger ones have since been constructed. The figure displays the growth in size, beginning with T1 and T2. These were built following a concept which originated at the National Research Council of Canada[25], and were experimental prototypes for T3. The two larger free piston shock tunnels, HEG[26] and HIEST[27], were constructed and are operated in government laboratories. At the top of Fig. 7(b) are two free piston expansion tubes which, as discussed below, are being developed for hypervelocity aerodynamics research.

Operating nozzle reservoir pressure levels for HEG and HIEST are 100MPa and 150MPa respectively, while both HEG and HIEST use nominal Mach 8 nozzles for scramjet engine testing, with exit diameters of 0·6m and 0·8m respectively. Figure 1 indicates that, by reducing the shock tunnel nozzle throat size, both of these facilities could provide simulation of propulsive flow fields up to test section Mach numbers exceeding 11.

In what may be regarded as the more conventional type of reflected shock tunnel, the driver gas is statically contained in the driver tube before rupture of the diaphragm at the entrance to the shock tube. This type of shock tunnel has found some use for testing scramjet configurations, but has been used mainly for aerodynamic research and development, and will be discussed in more detail below.

4.2 Instrumentation

Techniques of surface pressure and heat transfer measurements are well established and are widely used in shock tunnels for studies of propulsive flows. Schlieren and interferometric techniques of flow visualisation are also commonly used, and are particularly useful in impulse facilities because light sources which illuminate and allow recording of the field of view in less than one microsecond are readily available, making it a relatively straightforward matter to obtain images of the flow field.

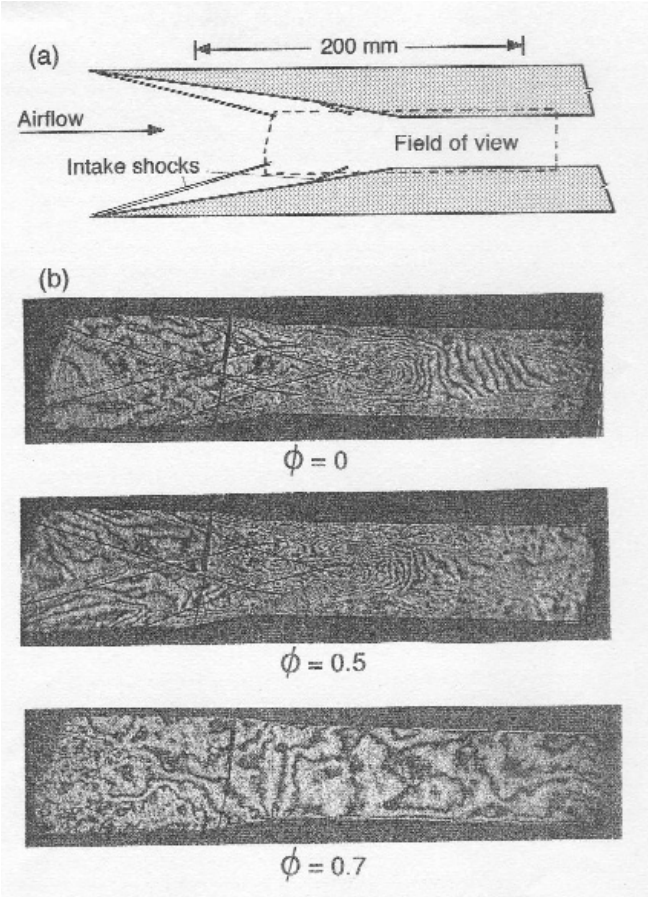


Figure 8. Holographic interferograms of supersonic combustion with hydrogen fuel. (a) Model configuration
(b) Flow patterns with fuel addition (ϕ = equivalence ratio, stagnation enthalpy = 3 MJ/kg, free-stream Mach number, pressure and temperature = 6·8, 8kPa and 290K respectively).

4.2.1 Interferograms

Holographic interferograms, obtained in shock tunnel T4, of a flow field with hydrogen combustion are displayed in Fig. 8[28]. As shown in Fig. 8(a), the model was a symmetric two dimensional duct with intake ramp angles of 9 degrees, followed by ramps of 12 degrees, leading to a combustion duct with parallel walls. The model flow path was 75mm wide, and fuel injection wall orifices were located 95mm downstream of the leading edges. Glass sidewalls allowed interferometric flow visualisation during the test time, a crack in one of these walls appearing as a black line roughly transverse to the flow near the upstream end of the combustion duct. Black lines are also used to show the theoretical location of the shocks from the intake, together with their interaction near the combustion duct entrance, for the no fuel injection case ($\phi = 0$) and the case of hydrogen injection at an equivalence ratio of 0·5. This part of the flow structure differs only a little between these two cases. However, differences become more apparent further downstream, where the fuel on interferograms show fringes which are more widely spaced and less structured in the zones near the walls, consistent with the occurrence of combustion heat release. At an equivalence ratio of 0·7 the flow is choked, and the hot subsonic flow shows widely spaced fringes, indicative of reduced density gradients, and the lack of structure associated with large scale turbulent eddies.

https://doi.org/10.1017/S0001924000004346 Published online by Cambridge University Press

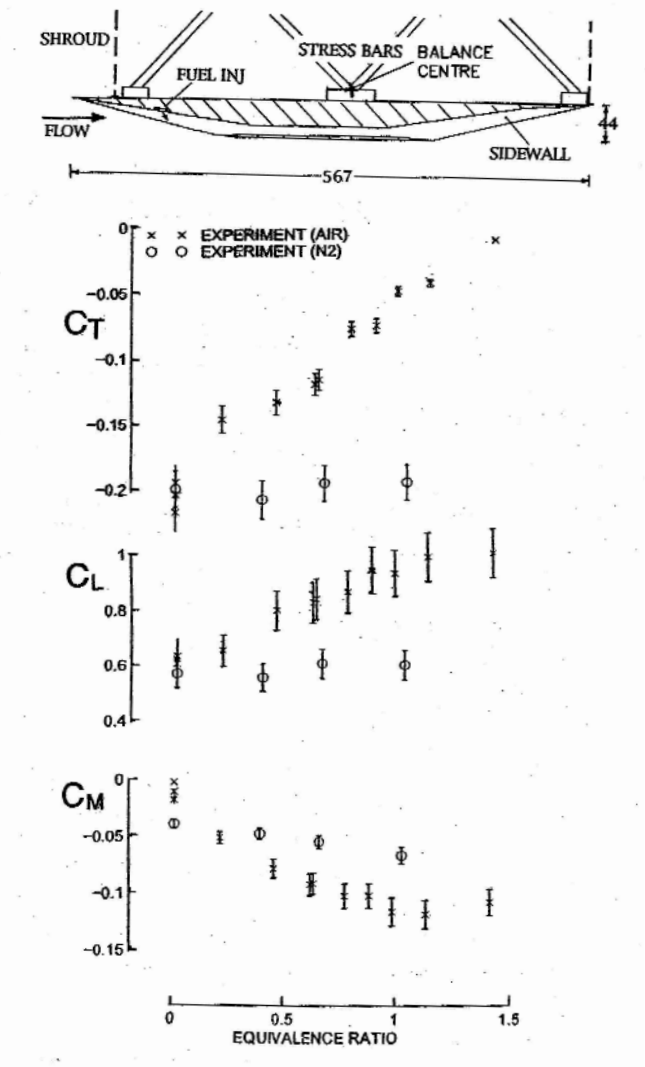


Figure 9. Scramjet Model Forces Measured by Stress Wave Force Balance (C_T = forward thrust coeff, C_L = lift coeff, C_M = nose up pitching moment coeff. about balance centre, Stagnation enthalpy = 3·3 MJ/kg, free stream Mach number, pressure and temperature = 6·6, 7kPa and 350K respectively. Dimensions of model in mm).

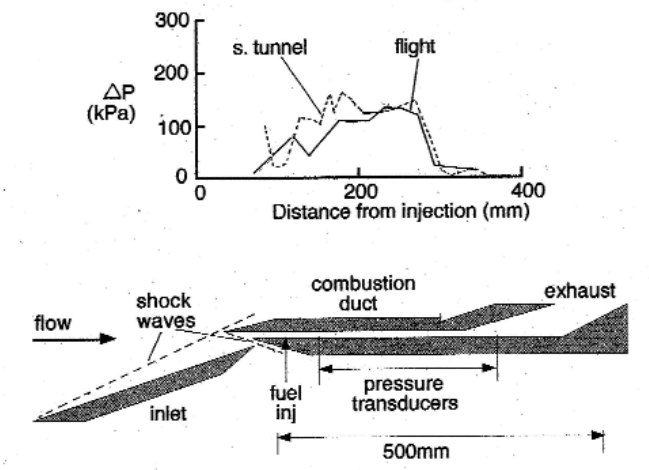


Figure 10. Supersonic combustion – shock tunnel vs Flight (ΔP = pressure increase due to hydrogen injection and combustion, equivalence ratio = 0·32 ± 0·02).

4.2.2 Model forces

The measurement of overall model forces is an important function of any wind tunnel, and this is also true of impulse wind tunnels. For a relatively 'clean' configuration, a general working rule is that the flow about a model closely approaches the steady state by the time that the steady mainstream has passed three model lengths, signifying that the overall forces acting on the model also become steady in that time. However, stress waves are induced in the model by transient starting loads, and these stress waves propagate in a normal steel or aluminium model with a speed which is of the order of the free stream flow speed, reflecting and re-reflecting as they traverse back and forth along the model. This leads to a situation where, although the forces acting on the model have reached a steady state, the internal stress distribution has not, and the magnitude of the steady state forces cannot be transmitted to a recording transducer. However, this problem can be circumvented by using the stress wave force balance technique[29]. This technique involves recording the stress waves passing into the model support struts during a test, and subsequently deconvoluting those records to obtain the timewise variation of forces on the model.

Figure 9 displays measurements of thrust, lift and pitching moment on a simple hydrogen fuelled scramjet configuration[30], obtained with a stress wave force balance in shock tunnel T4. The thrust is negative, indicating a net drag which only approaches zero as the equivalence ratio exceeds one but, as revealed by comparison with results obtained with nitrogen test gas, there is a substantial thrust increment due to combustion. There is also a considerable increment of lift due to combustion, and a substantial increase in the nose down pitching moment.

It is worth noting that the stress wave force balance technique can be used in impulse flows of duration much less than the one millisecond or so which is typical of shock tunnels. For example, it has been used successfully to measure the drag on cones in a small expansion tube with test times of 50 microseconds[31].

Provided that models are not too large, model forces can also be measured in shock tunnels with test times in excess of approximately 2 milliseconds by strain gauge balances, sometimes combined with accelerometers mounted in the model. A useful discussion of this type of force balance is given in Ref. 32.

4.2.3 Skin friction

Hypersonic propulsion will involve slender vehicles, and skin friction can be expected to constitute a major component of drag on such vehicles. Therefore, particular significance attaches to the measurement of skin friction in impulse facilities. A skin friction gauge, which used piezoelectric sensing elements in bending mode, was developed at the Cornell Aeronautical Laboratory in the 60s. This gauge had a natural frequency of 5kHz, and was used in an extensive shock-tunnel study of flat plate turbulent boundary layers[33]. A skin friction gauge was also developed at the University of Queensland. This gauge employed a piezoelectric element in direct shear mode, and had a natural frequency of 40kHz[34]. Gauges of this type were used in experiments which showed that combustion of hydrogen in a turbulent boundary layer reduced the skin friction by a factor of approximately three, and also reduced the heat transfer[35].

4.3 Flight – shock-tunnel comparison

Airbreathing propulsion at high speeds involves supersonic combustion and, though theoretical and experimental research has been done on supersonic combustion for some decades, no flight data existed which would allow a correlation between flight and wind tunnel research to be established. Thus the flight of a supersonic combustion experiment on a sounding rocket in July 2002[36], had particular significance.

https://doi.org/10.1017/S0001924000004346 Published online by Cambridge University Press

The flowpath of the experimental model is shown schematically in Fig. 10. It was fuelled with hydrogen, and involved a simple two shock inlet with the inlet ramp terminated before the combustion duct entry, as shown, in order to dump the inlet ramp boundary layer and the shock reflected from the cowl leading edge. Lateral dumps were also incorporated, thereby ensuring that the flow entering the 75mm wide and 9·8mm high rectangular combustion duct was uniform and parallel to the walls of the duct. The flight model had two identical flow paths, one of which was fuelled and the other unfuelled, thus allowing the pressure increase due to hydrogen injection and combustion to be determined at each moment during the flight experiment. The model for testing in the shock tunnel, T4, had only one flowpath, the fuel on and fuel off data being obtained in separate tests. Resulting distributions of pressure increase in the combustion duct due to hydrogen injection and combustion are compared at the top of the figure. The sounding rocket followed a parabolic trajectory, reaching an altitude of 320kilometres, and the experiment took place as the model re-entered the atmosphere, on an approximately vertical path, at a Mach number of 7·6.

The flight distribution of the pressure increase due to fuel injection shown in Fig. 10 was taken at an altitude of 29km, and is compared with the distribution obtained in the shock tunnel, before the flight, at conditions which simulated this altitude[37]. The shock tunnel distribution displays irregularities which are thought to result from marginal non-uniformities in the test flow (the shock tunnel nozzle was operated somewhat off design) but, disregarding these irregularities, it is almost the same as the flight distribution. This level of similarity between tunnel and flight distributions persisted at all other conditions experienced in the flight experiment, ranging from conditions where the flow was dominated by the chemical kinetics of combustion, to where mixing effects dominated. It indicated that, at least at stagnation enthalpies near 3MJ/kg, flight flow fields with combustion can be satisfactorily simulated in shock tunnels.

Following the success of the shock tunnel in predicting combustion in flight at Mach 7·6, the shock tunnel described in Ref. 16 was used to develop the combustor for the second successful flight of a NASA 'Hyper X' vehicle in November, 2004, when a Mach number of 9·7 was achieved.

5.0 IMPULSE WIND TUNNELS AND REYNOLDS NUMBER

While the primary purpose of developing impulse wind tunnels was to increase the velocities at which flight flow fields could be simulated, the relative simplicity of the wind tunnels which evolved encouraged design for relatively high pressure levels, with the result that impulse wind tunnels could be used to produce higher Reynolds numbers at a given Mach number than intermittent wind tunnels. Figure 11(a) illustrates the benefit of higher nozzle reservoir pressures, showing that they may be used to increase the test flow unit Reynolds number or, alternatively, to increase the test flow Mach number at a constant unit Reynolds number.

Figure 11(b) is a diagrammatic representation of three types of impulse wind tunnel which have seen regular use in the high Reynolds number/high Mach number mode[38,39,40]. The reflected shock tunnel uses the rupture of a high pressure diaphragm to initiate the unsteady expansion of driver gas from the high pressure reservoir, and thus to drive a shock wave through the test gas, as shown. Reflection of this shock wave from the downstream end of the shock tube produces the quasi-steady reservoir of test gas which supplies the nozzle flow. Mixing at the interface between the driver gas and test gas is a basic disadvantage of the reflected shock tunnel, as it limits the test time, and will be discussed below.

The gun tunnel uses the same basic configuration as the reflected shock tunnel, but employs a light piston to separate the driver gas from the test gas. The need to maintain the integrity of the piston

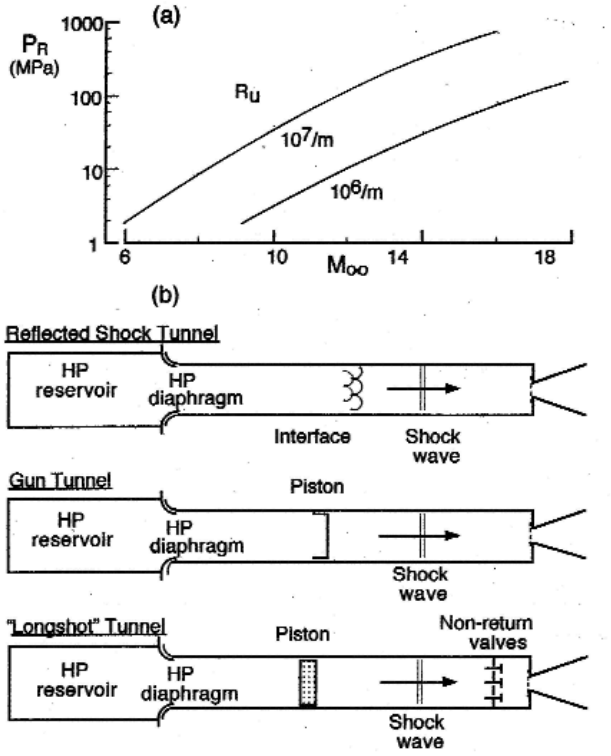


Figure 11. Impulse wind tunnels for high Mach numbers with high Reynolds numbers.
(a) Effect of nozzle reservoir pressure on test test section unit Reynolds number. (Ratio of specific heats = 1·35, test flow temperature = 90K, P_R = nozzle reservoir pressure, M_∞ = test flow Mach number, R_u = test unit Reynolds number).
(b) Typical high Reynolds number impulse wind tunnels.

dictates a minimum allowable piston mass and, because of this finite mass, the piston undergoes some oscillations as its compression stroke is completed. However, these oscillations are rapidly damped, and the ensuing test time is much longer than the test time of the reflected shock tunnel, ranging from 5 to 50 milliseconds. Test section velocities are limited to less than 2kms^{-1}. Gun tunnels are operated mainly as university research wind tunnels, where their simplicity and economy of operation is a particular advantage.

While the gun tunnel involves minimisation of the oscillations resulting from 'overshoot' of the piston as it completes its compression stroke, the 'longshot' wind tunnel seeks to maximise this overshoot, by using a moderately heavy piston, and trapping the test gas at high pressure by an array of non-return valves near the downstream end of the shock tube. In this way nozzle reservoir pressures in excess of 200MPa are obtained at high Mach numbers, yielding high values of the unit Reynolds number.

6.0 HYPERVELOCITY IMPULSE WIND TUNNELS

6.1 Blowdown reflected shock tunnels

The hypervelocity regime may be defined by flow velocities in excess of 3kms^{-1} and, by the use of appropriate driver gases, the blowdown (or conventional) reflected shock tunnel (illustrated schematically in Fig. 11(b)) is able to penetrate well into this regime.

https://doi.org/10.1017/S0001924000004346 Published online by Cambridge University Press

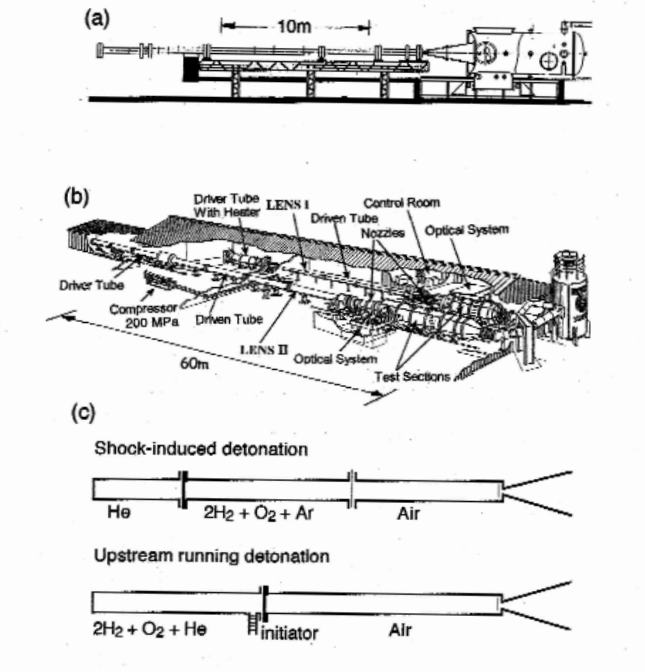


Figure 12. Blowdown hypervelocity reflected shock tunnels.
(a) shock tunnel TH2 (Ref. 41)
(b) The LENS shock tunnel facility (Ref. 42)
(c) Detonation drivers

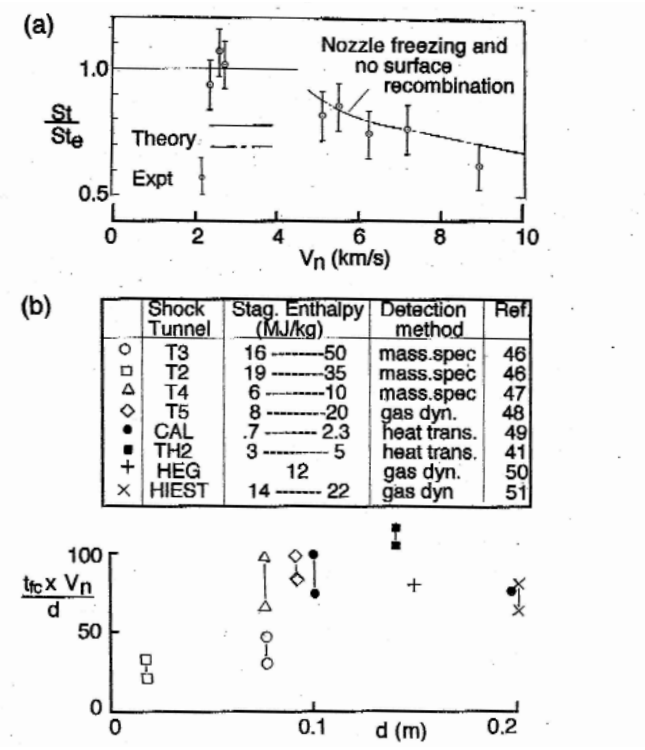


Figure 13. Hypervelocity performance of free piston shock tunnels.
(a) Production of hypervelocity flows in shock tunnel T3.
(St = Stanton number, St_e = Stanton number for no dissociation, $V_n = \sqrt{2H}$, H = stagnation enthalpy).
(b) Driver gas contamination of test flow (t_{fc} = test section contamination free time, d = shock tube diameter. Filled symbols indicate blowdown shock tunnels, remainder free piston driver).

Helium driver gas

An example of a blowdown hypervelocity reflected shock tunnel using helium driver gas is shown in Fig. 12(a)[41]. The shock tube and the driver have an internal diameter of 140mm, and are designed for pressures of 150MPa. An electrical resistance heater can raise the temperature of the helium driver gas to 500K before a test. This shock tunnel can reach test flow velocities of approximately 3·5kms^{-1}.

Hydrogen driver gas

higher test flow velocities are available with the LENS (large energy national shock tunnel) facility[42], shown in Fig. 12(b). The LENS I blowdown shock tunnel is designed for the use of hydrogen driver gas, and can reach test flow velocities of 5kms^{-1} by electrical heating of the driver gas. It has a 200mm diameter shock tube and a 280mm diameter driver, which has a design operating pressure of 200MPa, to yield a nozzle reservoir pressure of approximately 100MPa. Referring to Fig. 11, this allows test section Mach numbers of 16 with a unit Reynolds number of 10^6/m which, since this shock tunnel is able to accommodate models that are 4m in length, corresponds to a test section Reynolds number of 4×10^6 . This is the approximate value of the free stream Reynolds number associated with re-entry of the NASA Space Shuttle at a Mach number of 16.

The useable test flow diameter is 1m, implying that the value of the binary scaling parameter required for simulating flows with non-equilibrium dissociation can readily be produced in LENS I. Referring to Fig. 2, a test flow diameter and model length of 1m yields a test section pitot pressure of approximately 40kPa at a velocity of 5kms^{-1} which, at a test flow Mach number of 12, can be readily accommodated with a nozzle reservoir pressure of 60MPa. Investigations of dissociation effects in LENS I, focussing particularly on shock induced separated regions, are reported in Ref. 42.

Reflected shock tunnels normally are constrained to operate at hypersonic Mach numbers because the supply of shock heated gas at the nozzle entrance is only sufficient to sustain the test gas mass flow for the test period through a relatively small nozzle throat, implying that a given test flow area can only be supplied at Mach numbers greater than some minimum value. For LENS I, this minimum value of Mach number is 7. Lower test Mach numbers, ranging from 7 to 3, are obtained in LENS II, which has a 620mm diameter shock tube and driver. It uses helium driver gas and, since it is limited to test velocities of approximately 2kms^{-1}, it is not a hypervelocity facility when operated as a reflected shock tunnel. However, velocities of approximately 4·5kms^{-1} are obtained when LENS II is operated as LENS X, which is an expansion tube/tunnel variant of the LENS II assembly. Expansion tube operation is discussed below.

The development role of the LENS facilities is evident in their use for large scale testing of scramjet engines, and for aerothermal and aero-optic design of advanced missile seekerheads, as well as the seeker window obscuration problems presented by the proximity of manoeuvring thrusters. This development role is conducted together with basic research in areas such as shock–boundary–layer interactions and film cooling.

Detonation drivers

There was a period, particularly during the 1960s, when combustion of an oxyhydrogen mixture in helium driver gas was favoured as a means of producing hypervelocity test flows. It was then considered desirable to avoid detonation in these combustion drivers. Although this type of driver has fallen out of favour, combustion drivers involving exploitation of the detonation process have appeared during the last decade. They are not strictly blowdown drivers, as they are not in a static mode immediately prior to operation of the shock tunnel, but detonation drivers have been used as a means of

https://doi.org/10.1017/S0001924000004346 Published online by Cambridge University Press

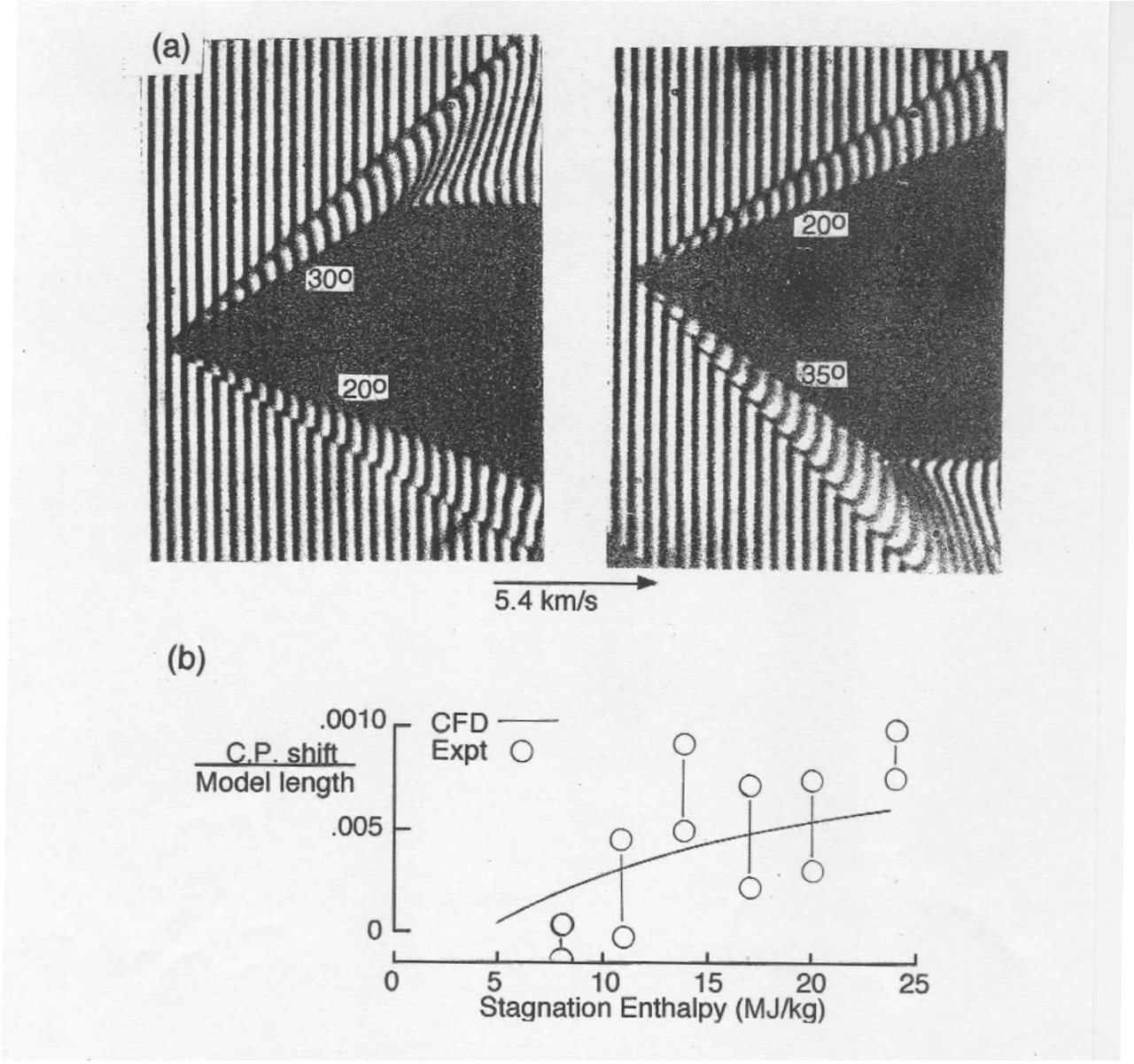


Figure 14. Effects of Nonequilibrium Dissociation reactions in hypervelocity flows.
(a) Mach Zehnder interferograms of wedge flows with dissociative relaxation.
(b) Centre of pressure shift on a model of reentry glider HOPE.

improving the performance of blowdown shock tunnels, and therefore are included here.

Figure 12(c) illustrates schematically two variants of the detonation driver. The shock-induced detonation driver uses the expansion of high pressure gas to drive a detonation wave through the oxyhydrogen in argon mixture when the high pressure diaphragm (shown in Fig. 12(c) as a thick line) bursts. The detonation mixture is restrained by a light diaphragm (shown by a thin line) which bursts on arrival of the detonation wave, to propagate a shock wave in the shock tube. This shock wave bursts a light diaphragm at the entrance to the nozzle to initiate the test flow. A detonation driver of this type has been used to increase the test flow stagnation enthalpy from less than 2MJ/kg with a room temperature helium driver alone to 5MJ/kg with the detonation driver incorporated[43].

The other variant is the upstream running detonation driver. It employs only one driver chamber which, as shown in Fig. 12(c), is filled with an oxyhydrogen helium mixture. The detonation is initiated at, or close to, the high pressure diaphragm by a suitable source (such as an electric arc or an auxiliary shock tube), and travels upstream. The pressure rise due to detonation bursts the high pressure diaphragm, and a shock wave propagates through the air in the shock tube to reflect and produce the nozzle flow. This type of driver has been used to generate test flows with a velocity approaching 5kms^{-1} in the shock tunnel of Fig. 12(a)[44].

6.2 Free piston reflected shock tunnels

As shown in Fig. 6(b), the driver gas temperature in a free piston shock tunnel increases with the driver gas volumetric compression ratio. Since the maximum stagnation enthalpy which can be produced in a reflected shock tunnel depends on the driver gas temperature, and since there is, in principle, no limit to the volumetric compression ratio which can be used, there is also no limit to the stagnation enthalpy which can be produced. In fact,

https://doi.org/10.1017/S0001924000004346 Published online by Cambridge University Press

driver gas contamination of the test gas and radiation of energy from the reflected shock region both tend to set upper limits to the stagnation enthalpy. Nevertheless, as shown by flat plate heat transfer measurements[45] in Fig. 13(a), stagnation enthalpies corresponding to Earth orbital velocity can be produced. The experimental Stanton numbers are consistent with predictions, which do not involve dissociation effects, at low stagnation enthalpies. They remain consistent at high stagnation enthalpies if the predicted Stanton number is calculated assuming that the composition of the boundary layer airflow remains frozen at the free stream dissociation levels, and the dissociated atoms do not recombine at the surface.

Driver gas contamination

driver gas contamination of test gas is usually the factor which limits the test time in a reflected shock tunnel. Figure 13(b) displays measurements of the test section contamination free time with helium driver gas for a number of shock tunnels. This contamination free time is the time between arrival of the first element of flow at the test section and arrival of contaminated flow. Therefore the useable test time is obtained by subtracting the nozzle flow starting time from the test section contamination free time. For the purpose of comparing shock tunnels, the product of contamination free time and the approximate flow velocity is taken, to yield a contamination free flow length, and normalising this by the diameter of the shock tube. Because dissociation freezing reduces the test section velocity, the contamination free flow length will be reduced by up to 20% at high stagnation enthalpies. As shown in the table in Fig. 13(b), a variety of techniques are used for detecting contamination. The gas dynamic technique involves choking of a small duct as the contamination rises above a preset level[48,52] and, together with the mass spectrometer, is able to detect contamination of 10% by molar concentration. The detection level using the heat transfer method is less well defined, but comparison with results from gas sampling probes indicate that the detection level is approximately 30%.

Figure 13(b) indicates that the contamination free flow length is directly proportional to the diameter of the shock tube, with the exception of the smaller shock tubes at high stagnation enthalpies. The operating conditions with T2, the smallest shock tube, suggested that the shorter test times may be due to the predominance of laminar boundary layers in the shock-tube, while the relatively extended test times with T4 may be due to use of a helium/argon driver gas mixture in this case. The results with shock tube diameters of 0·1m and greater indicate that there is not a significant difference between the contamination free flow lengths obtained with blowdown drivers and free piston drivers. In view of the similarity of the shock tube processes involved, this is not surprising.

Recognising the need to maximise the useable test flow length in reflected shock tunnels, there is a benefit to ensuring that the flow starting processes pass through the nozzle as quickly as possible. Since a substantial part of the starting time can be expected to occur near the throat, where the speed of the upstream propagating rarefaction wave which terminates the nozzle starting process most closely matches the flow velocity, the length of the supersonic region, near the nozzle throat, should be minimised. This implies that minimal starting time losses can be expected with a contoured nozzle employing the maximum divergence angle near the throat.

Dissociating hypervelocity flows

Examples of effects arising from the dissociation of air at hypervelocities are shown in Fig. 14. Mach Zehnder interferograms of wedge flows in the free piston shock tunnel T3 at a stagnation enthalpy of 19MJ/kg, a free stream total enthalpy, h_∞, of 4·5MJ/kg, and a pitot pressure of 320kPa, are displayed in Fig. 14(a). The two models shown were part of one model array in the shock tunnel, thus ensuring that they both experienced the same test flow. With a span which was six times the length of the 30° face shown, they produced wedge flows which were essentially two dimensional. The Mach Zehnder interferometer was manipulated to set a pattern of fringes across the field of view in such a way that a downstream shift of these fringes indicated an increase in density.

On the 20° wedge faces a fringe shift occurs at the shock wave but, apart from a slight forward shift close to the surface, due to boundary layer effects, the fringes are closely parallel to those in the free stream, indicating that nearly constant density prevails in the shock layer. The post shock streamline enthalpy, h_s, is 8MJ/kg, and reference to Fig. 3(b) indicates that, indeed, only a very small change in density would be expected in this case. On the 30° face, a post shock streamline enthalpy of 10·5MJ/kg is obtained and the value of the binary reaction parameter, px/u, is 0·7 Pa.s at the downstream edge of the wedge face. The density change along shock layer streamlines will thus be approximately represented by the h_∞ = 5MJ/kg to h_s = 10MJ/kg curve in Fig. 3(b) and, since the streamline flow lengths at any station in the shock layer will increase in passing from the shock to the surface, so will the density and the fringe shift, and the fringes will no longer be parallel to those in the free stream. This is evident in Fig. 14(a). On the 35° wedge face, the streamline enthalpy is 12MJ/kg, and the binary reaction parameter has a value of 1·3Pas at the downstream edge of that face. Referring to Fig. 3(b) indicates that the streamlines close to the surface are approaching equilibrium, and the density changes less rapidly along a streamline. Thus, the fringes tend to become parallel to those in the free stream, as observed towards the downstream end of the wedge face in Fig. 14(a).

The increase in shock–layer density along streamlines implies a reduction in the shock angle with respect to the surface and an associated reduction in the pressure. Although this is a small effect, it can cause a significant upstream shift in the centre of pressure. A centre of pressure shift largely attributed to this effect has been measured in the free piston shock tunnel HIEST over a range of stagnation enthalpies on a model of the proposed Japanese delta wing re-entry glider, HOPE[27]. The results are shown in Fig. 14(b). The centre of pressure shift measurements were obtained from the measured pitching moment by using the numerically computed values for the normal force coefficient, and are seen to follow a trend similar to that numerically predicted. These measurements confirm that the effect of dissociation at hypervelocities can be measured on models of flight vehicles in the short test times available in shock tunnels.

7.0 SUPERORBITAL IMPULSE WIND TUNNELS

Superorbital wind tunnels are defined as those which generate test flows at stagnation enthalpies in excess of those corresponding to low Earth orbital velocity. Interest in such wind tunnels is stimulated by the development of planetary exploration, and the attendant possibility of Earth re-entry at speeds greater than 8kms^{-1}. As noted above, the penetration of this regime by reflected shock tunnels is likely to be limited by radiation loss of energy from the reflected shock region due to high ionisation levels. This was confirmed by studies of the radiation loss from argon test gas in the free piston shock tunnels T3 and T2[53, 54], and led to investigation of the non-reflected shock tunnel and the expansion tube as means of penetrating the superorbital regime other than the reflected shock tunnel.

7.1 Non-reflected shock tunnel with prior steady flow

The hypersonic non-reflected shock tunnel, which is shown schematically in Fig. 15(a), was first proposed in 1956[2], and has since been the subject of experimental evaluation[55]. The conventional method of starting the hypersonic nozzle flow, shown as the 'without PSF' case in Fig. 15(a), involves rupture of a thin diaphragm at the entrance to the nozzle, which is pre-evacuated. This is unsatisfactory for a high velocity shock tunnel, because the

https://doi.org/10.1017/S0001924000004346 Published online by Cambridge University Press

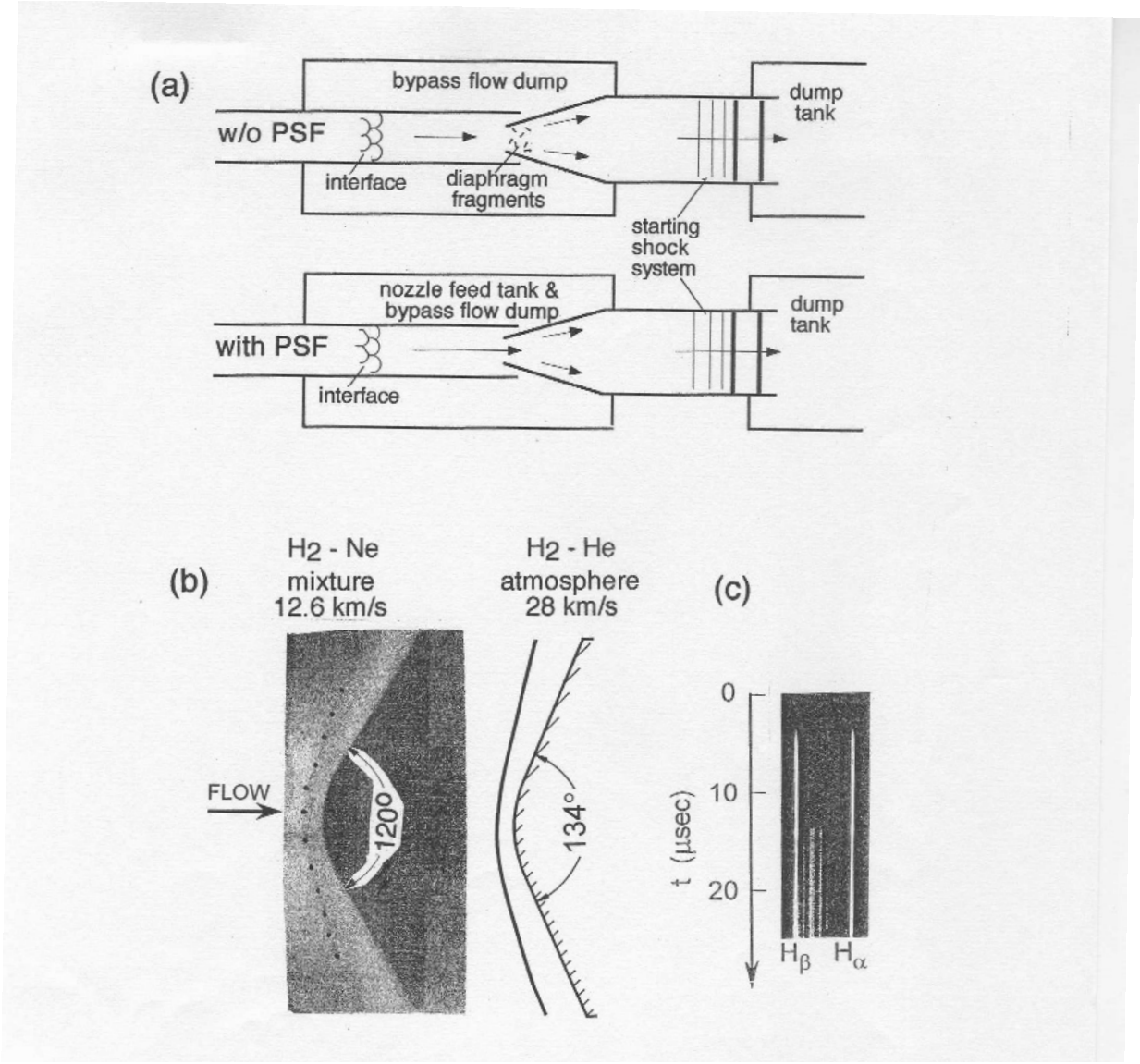


Figure 15. Prior Steady flow Nonreflected shock tunnel.
(a) Principle of operation (PSF = prior steady flow).
(b) Using hydrogen-neon mixture, at equivalent velocity 12·6kms^{-1}, to simulate shock layer at 28kms^{-1} in hydrogen-helium atmosphere. (Dots to help identify shock)
(c) Time resolved spectrum of radiation from stagnation region of a sphere in hydrdogen-neon mixture at equivalent velocity 14·8kms^{-1}.

inertia of any practical diaphragm is too large for it to be removed from the test flow in the few tens of microseconds of test time available in a high performance shock tube. The diaphragm can be rendered unnecessary by arranging that, immediately prior to a test, a steady flow of test gas is established in the nozzle[56,57]. This allows the nozzle starting process to be completed as rapidly as with a pre-evacuated nozzle and a massless diaphragm. The test gas necessary to replenish the loss of test gas from the shock tube to the prior steady flow is supplied by filling the bypass flow dump with test gas, allowing it to serve as a nozzle feed tank for the prior steady flow, and as a dump for the test gas which bypasses the nozzle during passage of the shock heated gas.

A modification to free piston shock tunnel T3 enabled it to operate as a prior steady flow non-reflected shock tunnel. Figure 15(b) shows a schlieren image of the shock wave on a spherically blunted cone obtained at conditions corresponding to entry into the atmospheres of Uranus or Neptune. The test gas was a mixture of 60% hydrogen with 40% neon, rather than the 85% hydrogen with 15% helium mixture which is more typical of the atmospheres of these planets, but it can be shown that both helium and neon act as inert diluents, and therefore that hydrogen-neon mixtures could be used to simulate ionising inviscid flow in hydrogen-helium atmospheres[58]. The density ratio across the shock wave is reduced by dissociation freezing of hydrogen in the nozzle, and this is taken into account to transform the shock and body shape of the 120° cone of the experiments into the 134° cone and associated shock shape of an undissociated free stream, as shown in Fig. 15(b). Thus, while the experiments were done in a hydrogen-neon test gas at an equivalent velocity of 12·6kms^{-1}, they provide a simulation of a flight velocity of 28kms^{-1} in a hydrogen-helium atmosphere.

Figure 15(c) displays a time resolved spectrum of the radiation from the shock layer in the stagnation region of a hemisphere at an

https://doi.org/10.1017/S0001924000004346 Published online by Cambridge University Press

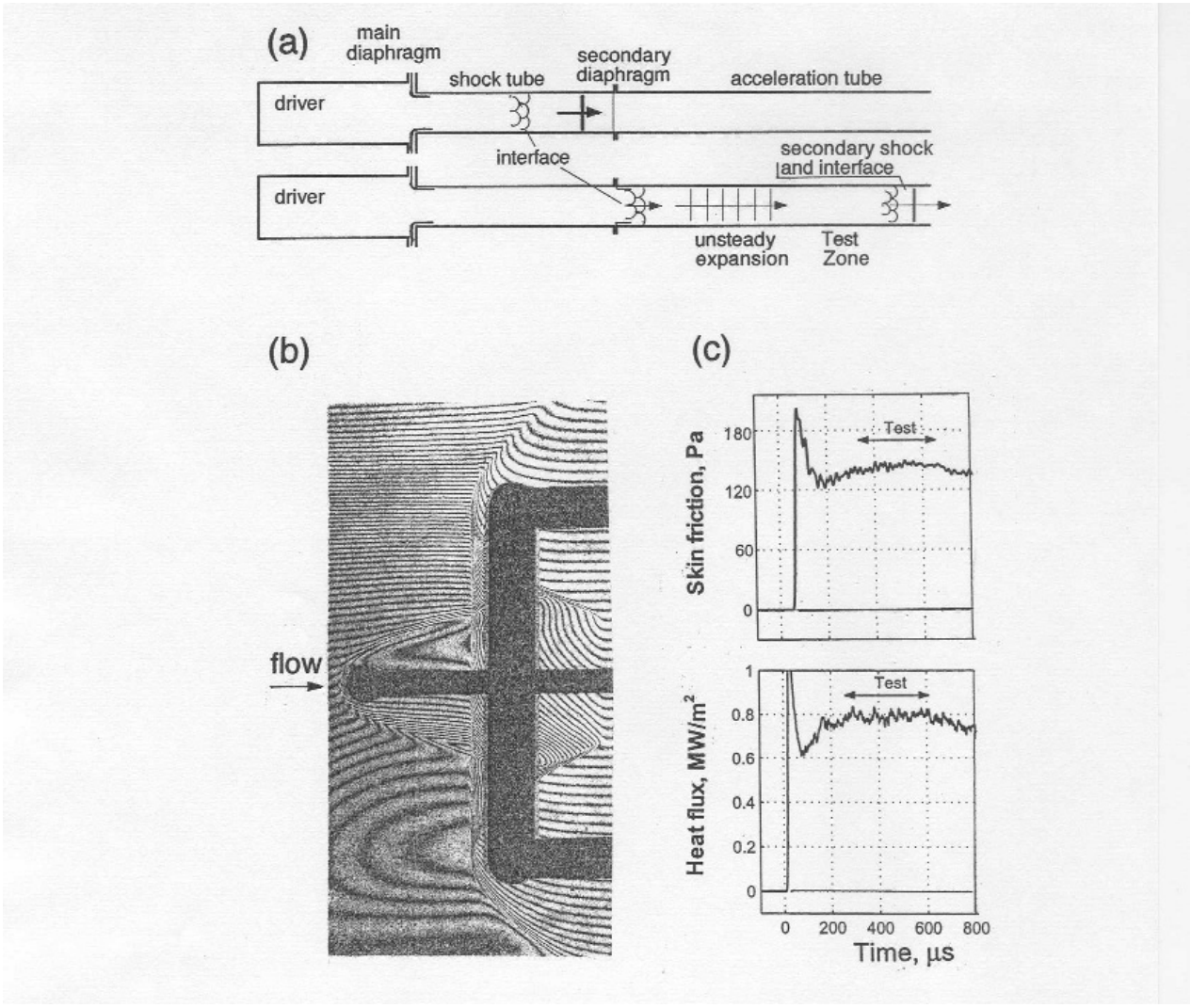


Figure 16. Expansion Tubes for Superorbital Flows.
(a) Producing test flow with an expansion tube.
(b) Interferometric flow visualization in X2 expansion tube test flow (H_2-Ne test gas, equivalent velocity 12·1kms^{-1}).
(c) Steady boundary layer flow in X3 expansion tube in N_2. (Duct length = 1·1 m, equivalent velocity = 8·7kms^{-1}, Ru = 3·1x10^5/m).

equivalent velocity of 14·8kms^{-1} and a Mach number of 6 in the above hydrogen-neon test gas. The time scale begins with the arrival of the starting shock system at the model. During the test period which follows, radiation over most of the visible part of the spectrum is seen to consist only of the H_α and H_β lines of hydrogen, before contact surface arrival is signalled by the appearance of other lines in the spectrum, which are ascribed to metallic diaphragm fragments at the contact surface. Thus removal of the diaphragm at the entrance to the nozzle has made it possible to produce a 'spectroscopically clean' hypersonic test flow.

The prior steady flow assembly can be designed to be interchangeable with the hypersonic nozzle of an existing reflected shock tunnel, thus offering the possibility of operation at higher stagnation enthalpies through the non-reflected mode.

7.2 Expansion tube/tunnel

The expansion tube, like the shock tunnel, is a variant of the shock tube but replaces the steady flow nozzle expansion with an unsteady expansion as a means of generating the final hypersonic test flow. The expansion tunnel adds a steady flow nozzle expansion of the hypersonic flow generated by the unsteady expansion.

The operation of an expansion tube is shown in Fig. 16(a). The top figure shows the shock tube in operation after rupture of the main diaphragm with the shock wave and following interface propagating towards a light secondary diaphragm at the downstream end of the shock tube. An acceleration tube follows the secondary diaphragm, and is initially at a lower pressure than the shock tube. The incident shock ruptures the secondary diaphragm, and is eliminated by the ensuing unsteady expansion wave, to produce the flow situation shown in the bottom of the figure, with the unsteady expansion and the interface passing downstream. A secondary shock is formed in the gas initially in the acceleration tube, together with a secondary interface between that gas and the test gas which has passed through the unsteady expansion. A region of uniform flow exists between the downstream end of the unsteady expansion and the secondary interface, thus forming a test region. Each element of gas in the unsteady expansion does work on the adjacent downstream element, with the result that the stagnation enthalpy and effective

https://doi.org/10.1017/S0001924000004346 Published online by Cambridge University Press

reservoir pressure of the test gas are increased in passing through the unsteady expansion.

Early attempts to develop operating expansion tube wind tunnels were only partly successful[59] because of the difficulty of eliminating large oscillations in the test section flow. A theoretical development by Paull[60] showed that this was due to lateral waves in the shock-tube driver gas, which were probably excited by bursting of the main diaphragm, and which tended to focus to a dominant frequency in passing through the unsteady expansion. These waves could be effectively prevented from passing through the shock tube interface by ensuring that the Mach number in the driver gas at the interface exceeded the Mach number in the test gas at the interface by a sufficient margin. Typically, this required a Mach number of 4 or 5 in the driver gas, a value which was reduced as the temperature of the driver gas increased. This theoretical development opened the way to the use of the expansion tube as a high velocity wind tunnel[61].

In addition to the free piston expansion tubes X2 and X3, shown in Fig. 7, Ref. 16 describes a blowdown shock tunnel which can also be reconfigured to operate as an expansion tube, while Ref. 62 describes a smaller blowdown expansion tube used for combustion studies. As mentioned in Section 6.1, the blowdown shock tunnel LENS II can also be reconfigured as an expansion tube which, by operating with a nozzle attached at the downstream end of the acceleration tube, becomes the expansion tunnel LENS X. The large acceleration tube diameter of LENS X (610mm) yields a relatively long expansion tube test time of 2 milliseconds at a flow velocity of 4·5kms^{-1}.

As already noted, the effective reservoir pressure is increased by passage of the test gas through an unsteady expansion, with the result that the test flow conditions correspond to a value of P_R, the effective nozzle reservoir pressure, which exceeds the initial pressure in the expansion tube driver. This effect is partially offset by the need for some expansion of the driver gas in order to prevent the penetration of Paull type waves into the test flow but, since the ratio of P_R to the driver pressure increases with test flow Mach number, the need to avoid Paull waves only shifts the effective magnification of P_R to somewhat higher test flow Mach numbers. As an example of the magnifications achieved in practice, experiments with a small free piston driven expansion tube[63], with a main diaphragm burst pressure of 53MPa, produced a test flow with an effective reservoir pressure of 330MPa at an equivalent velocity of 14·7kms^{-1} and a Mach number of 6·7. The magnification of P_R is an important feature of expansion tubes since, as indicated by Fig. 1 and Fig. 2, it allows flow simulation at a higher Mach number in a facility of given size.

Examples of experiments using the free piston expansion tubes X2 and X3 are shown in Fig. 16(b) and Fig. 16(c). Figure 16(b) is a holographic interferogram obtained during an investigation of a proposal for a planetary aerocapture configuration(64), consisting of a large toroidal balloon which, like a parachute, is towed behind a vehicle to generate a large, decelerating, drag. For the X2 expansion tube model, the toroidal 'ballute' is represented by a metal ring, while a sphere was used to represent the spacecraft. The X2 expansion tube had an acceleration tube internal diameter of 85mm and the model, which had an overall diameter of 48mm, was tested in the free jet issued from the end of the acceleration tube. The test equivalent velocity was 12·1kms^{-1}, and the test gas was a 15% hydrogen with 85% neon mixture, to represent aerobraking in the atmosphere of Neptune. This yielded a test time of 30 microseconds. Interferograms such as Fig. 16(b) indicated that the flow through the toroid was not subject to choking, thus allowing interpretation of measurements of heat transfer in the stagnation region on the toroid.

Figure 16(c) displays records of skin friction and heat transfer obtained in the X3 free piston expansion tube. X3 is shown in Fig. 7. It employs a two stage free piston driver, by which a large piston in a relatively low pressure compression tube is used to launch a smaller, but more massive, piston in a relatively high pressure compression tube[65]. The internal diameter of the acceleration tube is 183mm, approximately 140mm of which is useable test flow, and tests are done in the free jet emerging from the end of the acceleration tube. The results displayed in Fig. 16(c) were obtained in nitrogen test gas on one wall of a rectangular duct with an 80mm × 100mm inlet and a length of 1·1m, at a flow velocity, Mach number, and unit Reynolds number of 8·4kms^{-1}, 11 and 3·1 × 10^5 respectively[66]. The skin friction and heat transfer records were obtained at 0·46m and 0·16m respectively from the leading edge, and are typical of records obtained along the duct. As indicated on the figure, the test period exceeds 300 microseconds, which corresponds to a flow length of 2·5m. Thus, with provision of a suitable nozzle (to eliminate expansion waves propagating from the edge of the free jet), X3 can be expected to provide steady viscous flows on models over 1m long which do not develop large, nearly two dimensional, separated regions.

8.0 CONCLUSION

The last few decades have seen the development of new wind tunnel techniques for simulating hypersonic flight at ever increasing velocities, and this review has focussed on these developments. The parallel development of computational fluid mechanics is outside the scope of the review, although the importance of computational fluid dynamics should be noted, not only for extrapolating from the wind tunnel to flight, but also for understanding the operation of these new wind tunnels themselves. The review has considered the wind tunnel simulation of propulsive flow fields and of hypervelocity aerodynamic flow fields, with some attention to the nascent area of superorbital aerodynamic flow fields.

A new feature of simulation of both propulsive and hypervelocity aerodynamic flow fields is a binary scaling requirement which, at a given free stream velocity and temperature, also implies a Reynolds number requirement. Binary scaling yields a nexus between wind tunnel size and operating pressure levels – as tunnel size is increased, lower reservoir pressures are required. For the hypervelocity case, this requirement may be compromised by a need to retain high reservoir pressures as a means of minimizing the effects of dissociation freezing in the hypersonic nozzle.

By burning the oxygen in air, and adding make-up oxygen, intermittent wind tunnels have been built which achieve velocities up to 2·5kms^{-1} with test times of at least a few seconds. The use of these wind tunnels for scramjet research and development, as well as for materials and thermostructural testing, is discussed. Also noted is an attempt to exceed test velocities of 2·5kms^{-1} with intermittent wind tunnels, without the need to vitiate the test gas, by using ultra high pressure technology combined with electron beam heating.

The velocity limit experienced by intermittent wind tunnels turned attention to the use of impulse wind tunnels, with test times of a few milliseconds. The consequential use of reflected shock tunnels for propulsive testing is outlined, with particular attention to free piston reflected shock tunnels. Examples are given of instrumentation used in shock tunnels for propulsive research.

A brief account is given of the 'HyShot' supersonic combustion flight experiment. This is an important development, as it demonstrates the existence of a reasonably economical path from the laboratory to flight status of a hypersonic vehicle.

A brief discussion of the use of shock tunnels and their variants as high Reynolds number hypersonic wind tunnels is followed by consideration of their dominant role in hypervelocity simulation. The LENS facility is described, as a particularly impressive example of blowdown shock tunnels which can operate in the suborbital hypervelocity regime, before turning attention to free piston shock tunnels, and the role of driver gas contamination in limiting test times in reflected shock tunnels. It is shown that stagnation enthalpies throughout the suborbital regime are available with free piston shock tunnels, and observations at high stagnation enthalpy which display

https://doi.org/10.1017/S0001924000004346 Published online by Cambridge University Press

the effects of dissociative relaxation on hypervelocity model flows in air are described.

Finally, results of experiments in two types of superorbital impulse wind tunnels are displayed. The experiments show that the prior steady flow non-reflected shock tunnel can produce the high stagnation enthalpies required, and that the expansion tube can also produce those stagnation enthalpies, but with a test time which is an order of magnitude longer.

This review illustrates the degree to which aerodynamic ground testing will increasingly rely on hypersonic impulse wind tunnels as velocities increase, and impulse wind tunnel instrumentation is further developed. Intermittent wind tunnels can be expected to continue to play an important role, particularly in areas such as engine and vehicle systems, and thermo-structural testing, but the difficulty of making a high velocity wind tunnel with test times of at least a few seconds will encourage reliance on impulse wind tunnels, coupled with judicious and economical use of flight testing.

REFERENCES

1. BAALS, D.D. and CORLISS, W.R. Wind tunnels of NASA, NASA SP-440, 1981, pp 81-87.
2. HERTZBERG, A. The application of the shock tube to the study of the problems of hypersonic flight, *Jet Propulsion*, 1956, **6**, (7), pp 549-554.
3. WITTLIFF, C.E., WILSON, M.R. and HERTZBERG, A. The tailored-interface hypersonic shock tunnel, *J Aerospace Sci*, 1959, **26**, (4), pp 219-228.
4. NAGAMATSU, H.T., GEIGER, R.E. and SHEER, R.E.(Jr), Hypersonic shock tunnel, *ARS Journal*, 1959, **29**, (5), pp 332-340.
5. LACEY, J., INOUE, Y., HIGASHIDA, A., INOUE, M., ISHIZAKA, K. and KORTE, J.J. Mach 10 Hypersonic nozzle: improved flow quality, *J Spacecraft and Rockets*, 2003, **40**, (1), pp 126-131.
6. MERSKI, N.R. Global aeroheating wind-tunnel measurements using improved two-color phosphor thermography method, *J Spacecraft and Rockets*, 1999, **36**, (2), pp 160-170.
7. STALKER, R.J. and MORGAN, R.G. Supersonic hydrogen combustion with a short thrust nozzle, *Comb and Flame*, 1984, **57**, pp 55-70.
8. PAULL, A. Hypersonic ignition and thrust production in a scramjet, AIAA Paper No. 93-2444. Presented at AIAA/SAE/ASME/ASEE 29th Joint propulsion conference, Monterey, CA, USA, 28-30 June 1993.
9. STALKER, R.J. and PULSONETTI, M.V. Experiments on scaling of supersonic combustion, Univ. of Queensland, Mechanical Engineering Research Report No 2004/3, 2004.
10. WITTLIFF, G.E., SUNDARAM, T.R., RAE, W.J. and LORDI, J.A. Study of high density hypervelocity flows and similitudes, AEDC Rep, TR-67-72. Arnold Eng Dev Center, Tullahoma, Tenn, USA, 1967.
11. STALKER, R.J. Approximations for nonequilibrium hypervelocity aerodynamics, *AIAA J*, 1989, **27**, (12), pp 1761-1769.
12. HAYES, W.D. and PROBSTEIN, R.F. *Hypersonic Flow Theory*, 1st Ed., New York, Academic Press, 1959, pp 24-26.
13. HARRIS, C.J. Comment on nonequilibrium effects on high-enthalpy expansion Of air, AIAA J, 1966, (**4**). 6, p 1148.
14. STALKER, R.J. Hypervelocity aerodynamics with chemical nonequilibrium, *Ann. Rev. Fluid Mech*, 1989, **21**, pp 37-60.
15. CHASE, R.L. and TANG, M.H. A History of the NASP Program from the formation of the joint program office to the termination of the HySTP Scramjet Performance Demonstration Program, AIAA Paper No.95-6031, Presented at AIAA 6th Int Aerosp Planes and Hypersonics Technologies Conference, Chattanooga, TN, 3-7 April, 1995.
16. ROFFE, G., BAKOS, R., ERDOS, J. and SWARTWOUT, W. The propulsion test complex at GASL, AIAA Paper No. 97-7096, 13th Int Symp On Air Breathing Engines, Chattanooga, TN, 7-12 September 1997.
17. GUY, R.W., ROGERS, R.C., PUSTER, R.L., ROCK, K.E. and DISKIN, G.S. The NASA Langley Scramjet Test Complex, AIAA Paper No. 96-3243, Presented at 32nd AIAA/ASME/SAE/ASEE Joint Propulsion Conference, Lake Buena Vista, Fl, USA, 1-3 July, 1996.
18. GARRARD, D. and RIGNEY, S. Building for the Future – AEDCs investment in hypersonic aeropropulsion T & E, AIAA Paper No. 2000-2644, Presented at 21st AIAA Aerodynamic Measurement and Ground Testing Conference, Denver, CO, USA, June 2000.
19. MILES, R.B., BROWN, G.L., LEMPERT, W.R., YETTER, R., WILLIAMS, G.J. JR, BOGDONOFF, S.M., NATELSON, D. and GUEST, J.R., Radiatively driven hypersonic wind tunnel, *AIAA J*, 1995, **33**, (8), pp 1463-1470.
20. BROWN, G.L., GIRGIS, I.G., JIANG, F. and LOCKNER, T.R. A review of the RDHWT/MARIAH II Fluid mechanics modeling and experiments, AIAA Paper No 2004-2481, 24th AIAA Aerodynamics measurement technology and ground testing conferences, Portland, OR, USA, 28 June – 1 July 2004.
21. COSTANTINO, M. and DARNELL, I. Ultra-high pressure modelling and experiments review, AIAA Paper No 12004-2482, 24th AIAA Aerodynamic Measurement Technology and Ground Testing Conference, Portland, OR, USA, 28 June – 1 July 2004.
22. TAMAGNO, J. and LINDEMAN, O. Experimental results on supersonic combustion general applied science laboratories, Ronkonkoma, New York, USA, December 1962.
23. OSGERBY, I.T. SMITHSON, H.K. and WAGNER, D.A., Supersonic combustion tests with a double-oblique-shock SCRAMjet in a shock tunnel, *AIAA J,* 1970, **8**, (9), pp 1703-1705.
24. STALKER, R.J. Development of a hypervelocity wind tunnel, *Aeronaut J*, 1972, **76**, pp 374-384.
25. STALKER, R.J. An Investigation of free piston compression of shock tube drive gas, Nat Res Council, Canada, Div of Mech Eng Report MT-44, May 1961.
26. GARDNER, A.D., HANNEMANN, K. STEELANT, J. and PAULL, A. Ground testing of the hyshot supersonic combustion flight experiment in HEG and Comparisonwith Flight Data, AIAA Paper No 2004-3345, 40th AIAA Joint Propulsion Conference, Ft. Lauderdale, Fl, USA, 11-14 July 2004.
27. ITOH, K., UEDO, S., TANNO, H., KOMURA, T. and SATO, K. Hypersonic aerothermo-dynamic and scramjet research using high enthalpy shock tunnel, *Shock Waves*, 2002, **12**, pp 93-98.
28. ODAM, J. Scramjet experiments using radical farming, PhD Thesis, The University of Queensland, Australia, November 2004.
29. SANDERSON, S.R. and SIMMONS, J.M. Drag Balances for Hypervelocity Impulse Facilities, *AIAA J*, 1991, **29**, (1), 2, pp 2185-2191.
30. ROBINSON, M.J. Simultaneous Lift, Moment and Thrust Measurements on a Scramjet in hypervelocity flow, PhD Thesis, University of Queensland, Austrlia, Dec 2003.
31. SMITH, A.L. and MEE, D.J. Drag measurements in a hypervelocity expansion tube, shock waves, 1996, **6**, pp 161-166.
32. STÖRKMANN, V., OLIVIER, H. and GRÖNIG, H. Force measurements in hypersonic impulse facilities, *AIAA J*, 1998, **36**, (3), pp 342-348.
33. HOLDEN, M.S. An experimental investigation of turbulent boundary layers at high mach number and Reynolds numbers, Cornell Aero. Lab Report No AB-5072-A-1. NASA CR-112147, November 1972.
34. GOYNE, C.P., STALKER, R.J. and PAULL, A. transducer for direct measurement of skin friction in hypervelocity impulse facilities, *AIAA J*, 2002, **40**, pp 42-49.
35. GOYNE, C.P., STALKER, R.J., PAULL, A. and BRESCIANINI, C.P. Hypervelocity skin-friction reduction by boundary-layer combustion of hydrogen, *J Spacecraft and Rockets*, 2000, **37**, (6), pp 740-746.
36. PAULL, A., ALESI, H. and ANDERSON, S. HyShot flight program and how it was developed, AIAA Paper No 2002-5248, 11th AIAA/AAAF International Space Planes and Hypersonic Sys & Tech Conference, Orleans, France, 29 September – 4 Oct 2002.
37. FROST, M.A. HyShot Scramjet Experiments in the T4 Shock Tunnel, M Eng Sc Thesis, University of Queensland, 2002.
38. HOLDEN, M.S. An Experimental Investigation of Turbulent Boundary Layers at High Mach Number and Reynolds Numbers, NASA CR-112147, November 1972.
39. BOYCE, R.R. and HILLIER, R. Shock-induced three-dimensional separation of an axisymmetric hypersonic turbulent boundary layer, AIAA Paper No. 2000-2226, Presented at 21st AIAA Aerodynamic Measurement and ground testing conference, Denver, CO, USA, June 2000.
40. STÖRKMANN, V., OLIVIER, H., GRÖNIG, H. and PARIS, S. Force measurement on ELAC Ia and on a Re-entry capsule in short duration hypersonic facilities, Proc 21st Int Symp on Shock Waves, Great Keppel Island, Australia, 20-25 July 1997, pp 563-568. A.F.P. HOUWING (Ed), Panther Publishing, ACT 2609, Australia.
41. GRÖNIG, H. Description of the Aachen shock tunnel TH2, Shock Wave Laboratory, Technical University Aachen, Templergraben 55, 5100 Aachen, January 1991.
42. HOLDEN, M.A., WADHAMS, T.P. and CANDLER, G.V. Experimental studies in the LENS shock tunnel and expansion tunnel to examine real-gas effects in hypervelocity flows, AIAA Paper No 2004-0916, 42nd AIAA Aerospace Sciences Meeting, Reno, NV, USA, 5-8 January 2004.

https://doi.org/10.1017/S0001924000004346 Published online by Cambridge University Press

43. BAKOS, R.J. and ERDOS, J.I. Optimizing pressure recovery in a detonation driven reflected shock tunnel, Proc 21st Int Symp on Shock Waves, Great Keppel Island, Australia, 20-25 July 1997, pp 1359-1365. HOUWING A.F.P. (Ed), Panther Publishing, ACT 2609 Australia.
44. GLÖßNER, C. and OLIVIER, H. Force and Moment Measurement on the HOPPER Configuration for High Enthalpy Conditions, Proc. 24th In. Symp. on Shock Waves, Beijing, China, 11-16 July 2004, pp 203-208. (Ed) ZIANG Z., Springer, Berlin.
45. EAST, R.A., STALKER, R.J. and BAIRD, J.P. Laminar flat plate heat transfer measurements from a dissociated high enthalpy hypersonic air flow, *J Fl. Mech*, 1980, **94**, pp 673-699.
46. SLADE, J.C., CRANE, K.C. and STALKER, R.J. Driver gas detection by quadrupole mass spectrometry in shock tunnels, Proc. 19th Int. Symp. on Shock Waves, Marseille, France, 26-30 July 1993, pp 293-298. BRUN R. and DIMITRESCU L.Z. (Ed), Springer, Berlin.
47. SKINNER, K.A. Mass spectrometry in Shock Tunnel Experiments of Hypersonic Combustion, PhD Thesis, University of Queensland, December 1994.
48. SUELANI, N. and HORNUNG, H.G. Detection and reduction of driver gas contamination in a high-enthalpy shock tunnel, Proc. 21st Int. Symp. on Shock Waves, Great Keppel Island, Australia, July 20-25, 1997, pp 543-548. Ed. HOUWING A.F.P., Panther Publishing, ACT 2609, Australia.
49. *Cornell Aeronautical Laboratory Hypersonic shock tunnel – Description and Capabilities,* May 1969. Cornell Aero. Lab. Of Cornell Univ, Buffalo, NY, 14221, USA.
50. HANNEMANN, K. Inst. of Aerodyn. And Flow Technology, Göttingen, Germany. Private Communication.
51. ITOH, K. National Aerospace Lab, Kakuda, Japan. Private Communication.
52. PAULL, A. A simple shock tunnel driver gas detector, 1996, *Shock Waves*, **6**, (5), pp 309-312.
53. HORNUNG, H.G. and SANDEMAN, R.J. Interferometric measurements of radiating ionizing argon flow over blunt bodies, *J Phys. D: Appl, Phys*, 1974, **7**, pp 920-934.
54. LOGAN, P.F., STALKER, R.J. and MCINTOSH, M.K. A shock tube study of radiative energy loss from an argon plasma, *J Phys D: Appl Phys*, 1977, **10**, pp 323-337.
55. OERTEL, H. Non-reflected shock tunnel test times, Prof. 7th Int. Shock Tube Symp, Toronto, Canada, June 23-25 1969, pp 80-1081. (Ed) GLASS I.I., Univ. of Toronto Press.
56. MUDFORD, N.R. and STALKER, R.J. The production of pulsed nozzle flow in a shock tube, AIAA Paper No 76-357. Presented at AIAA 9th Fl and Plasma Dyn Conference, San Diego, CA, July 1976.
57. STALKER, R.J. and MUDFORD, N.R. Unsteady shock propagation in a steady flow nozzle expansion, *J Fluid Mech*, 1992, **241**, pp 525-548.
58. STALKER, R.J. and EDWARDS, B.P. Hypersonic blunt-body flows in hydrogen-neon mixtures, *J Spacecraft and Rockets*, 1998, **35**, (6), pp 729-735.
59. MILLER, C.G. Operational experience in the langley expansion tube with various test gases, *AIAA J*, 1978, **16**, (3), pp 195-196.
60. PAULL, A. and STALKER, R.J. Test flow disturbances in an expansion tube, *J Fluid Mech*, 1992, **245**, pp 493-521.
61. NEELY, A.J., STALKER R.J. and PAULL, A. High enthalpy, hypervelocity flows of air and argon in an expansion tube, *Aeronaut. J*, 1991, **95**, (946), pp 176-186.
62. BEN-YAKAR, A. and HANSON, R.K. Characterization of expansion tube flows for hypervelocity combustion studies, *J Prop and Power*, 2002, **18**, pp 943-952.
63. NEELY, A.J. and MORGAN, R.G. The Superorbital expansion tube concept, experiment and analysis, *Aeronaut J*, March 1994, **98**, (973), pp 97-105.
64. MCINTYRE, T.J., LOUREL, I., EICHMANN, T.N., MORGAN, R.G., JACOBS, P.A. and BISHOP, A.I. Experimental expansion tube study of the flow over a toroidal ballute, *J Spacecraft & Rockets*, 2004, **41**, (5), pp 716-725.
65. MORGAN, R.G. Development of X3, a superorbital expansion tube, AIAA Paper No 2000-0558. Presented at 38th Aerospace Sciences Meeting, Reno, NV, January 2000.
66. SILVESTER, T.B., MORGAN, R.G. and JACOBS, P.A. Skin friction measurements in a duct in the X3 Superorbital Expansion Tube, AIAA Paper No 2004-3551. Presented at 40th AIAA/ASME/SAE/ASEE Joint Propulsion Conference, Ft. Lauderdale, FL, USA, July, 2004.

https://doi.org/10.1017/S0001924000004346 Published online by Cambridge University Press